ABSTRACT

KUDGUS, RACHEL A. Gold Nanoparticle Therapeutics: Disrupting Protein/Protein Interactions and the Treatment of Multidrug Resistant Pathogens. (Under the direction of Dr. Christian Melander).

Research with gold nanoparticles has exploded since the development of the Brust synthesis in 1994. Since that time, gold nanoparticles have been shown to be biologically inert, tunable in core size and monolayer, comparable in size to protein therapeutics and utilized as multivalent scaffolds. Attracted by the versatility of the gold nanoparticle, we investigated gold nanoparticles for combating multidrug resistance and enhancing the binding affinity of a known small molecule to a protein target.

The design and synthesis of multivalent gold nanoparticle antibiotics is presented. The thiolated penicillin derivatives **KDK-1022** and **EAK-223** were synthesized and conjugated to 2.0 nm diameter gold nanoparticles. Free **KDK-1022** and **EAK-223** were effective at inhibiting the growth of methicillin-susceptible *Staphylococcus aureus* (MSSA), but had little inhibitory effect on methicillin-resistant *Staphylococcus aureus* (MRSA). In contrast, **KDK-1022** and **EAK-223** conjugated to gold nanoparticles were active toward both MSSA and MRSA growth inhibition. Thus, when conjugated to gold nanoparticles, these lactam derivatives appear to be less susceptible to the resistance mechanisms that render the free molecules less effective. The results presented here suggest that multivalent display of small molecules on gold nanoparticles can convert resistance-compromised small-molecule drugs into potent nanoscale therapeutics.

We also describe the size comparability of a 2.0 nm gold nanoparticle to a 15 kDa protein and illustrate the conjugation and binding assays used to prove binding affinity can

be enhanced with the use of a multivalent scaffold. The multivalent character has the ability to turn a weak binding molecule into a stronger one through multiple contact points. In addition to this, increasing the size of the therapeutic could improve its ability to inhibit two proteins interacting via large surface area contacts (sterics). Specifically, the total footprint of the nanoparticle will be large enough to disrupt all contact points between the protein targets. To examine our hypothesis we employ the Interleukin – 2/Interleukin – 2 receptor interaction and a known small molecule that binds to Interleukin – 2. We describe synthesis of drug/gold nanoparticle conjugates, quantitation of drugs per particle, and demonstrate that drug coated nanoparticles bind interleukin-2 using Biacore, and Biacore evaluation to determine binding affinity.

Gold Nanocrystal Therapeutics: Treatment of Multidrug Resistant Pathogens and Disrupting Protein/Protein Interactions

by
Rachel A. Kudgus

A dissertation submitted to the Graduate Faculty of
North Carolina State University
in partial fulfillment of the
requirements for the Degree of
Doctor of Philosophy

Chemistry

Raleigh, North Carolina

2010

APPROVED BY:

_____	_____
Dr. Lin He	Dr. Elon Ison
_____	_____
Dr. David Shultz	Dr. Christian Melander, Chair

DEDICATION

I would like to dedicate this work to my parents, without them I never would have made it! They have always given me wings to fly and the courage and confidence to pursue any goal. They have also given me the encouragement, support and love required to achieve these goals.

BIOGRAPHY

The author, Rachel A. Kudgus, was born in Binghamton, NY on July 17th 1982 to Kathy and Eugene Kudgus. Rachel has three siblings, David, Rebecca, and Bethany. She spent her childhood growing up in Endwell, NY and graduated from Union-Endicott High School in 2000. After high school, Rachel attended Binghamton University where she received her Bachelors of Science in Chemistry in 2004. As an undergraduate, Rachel was a resident advisor for two years, and participated in undergraduate research for three years in Dr. Scott Handy's laboratory.

In the fall of 2004, Rachel began her graduate studies at Binghamton University and continued to work under the direction of Dr. Handy. In 2005, Rachel decided to follow her parents and move to North Carolina, where she subsequently re-started her graduate studies. At North Carolina State University, Rachel worked under the advisement of Dr. Christian Melander and worked closely with her collaborator, Dr. Daniel Feldheim at the University of Colorado at Boulder. Upon completion of her Ph.D. in 2010, she began a postdoctoral position at the Mayo Clinic in Rochester Minnesota under the direction of Dr. Priyabrata Mukherjee.

ACKNOWLEDGEMENTS

There are a countless number of people that have been a respected source of direction and support to this point in my life, and all of you have contributed to my achievement today. To begin with I would like to take this opportunity to thank Dr. Christian Melander. His passion, fire and dedication for his work have left a lasting impression on me. To all of my committee members, Dr. Lin He, Dr. Elon Ison, Dr. David Shultz, and Dr. Douglas Cullinan, thank you for taking the time for useful discussion and advice.

I would also like to thank my collaborators, Dr. Dan Feldheim and Dr. Chris Ackerson. They both opened by eyes to the nano world. Dr. Ackerson taught me the fundamentals I needed to begin in a new area of science and pushed me to become independent, even before I thought I was ready. To Dr. Dan Feldheim, I can not begin to find the words to thank you. The immeasurable number of hours we spent discussing science has shaped and prepared me for the future.

I must also thank all of the members, past and present, of the Melander and Feldheim groups. I have essentially spent equal time doing research in both labs, and have found scientists and friends that I will respect for a lifetime. I'd like to give a special acknowledgement to Dr. Christine Heinecke. We shared labs, offices and even an apartment, and admittedly there were times we couldn't stand each other, but I have no idea what I would have done without her. I'd like to also thank Carly Carter, in Raleigh and in Boulder; she was a source of support and friendship. Thank you both for the talks, scientific and

otherwise, and thank you for never making me drink alone. If we ever find ourselves in the same cities again, beers are on me.

Furthermore, I would like to recognize my family. I have two brothers (David, and Matt), four sisters (Rebecca, Bethany, Holly and Curly), two parents (Mom and Dad), and a dog (Molly), all of which I need to recognize and thank for their continuous help, advice, and support throughout this process. I love you all so very much. You have all contributed to helping me achieve my goals. Without the endless love, support, and encouragement I would not be here today. I will never forget that and I will forever be grateful to the extraordinary people I have been blessed to be able to call my family.

Lastly, I need to single out my parents. Mom and Dad you are always there for me. There to listen to me rant, cry or tell long stories about my research; there to hug me, to support me, to encourage me, and even to push me. I always wanted more because I could see it; you gave me visions and aspirations, and the nerve to go after it. I am so lucky to have the two of you in my corner. You have been there for the achievements and the pitfalls. You instilled the drive, persistence, and work ethic in me that is required to get here. I never would have made it without you; this is as much your accomplishment as it is mine. From the bottom of my heart, Thank you and I love you.

TABLE OF CONTENTS

Page

LIST OF TABLES viii

LIST OF FIGURES ix

LIST OF SCHEMES xii

LIST OF ABBREVIATIONS AND TERMS xiii

CHAPTER 1: Gold and Gold Nanoparticle 1

1.1. Gold through the Ages 1
1.2. Metal Nanoparticles 4
1.2.1. Synthesis 5
1.2.1.1. Citrate Reduction of Gold Nanoparticles 5
1.2.1.2. Brust Synthesis of Gold Nanoparticles 5
1.2.2. Modification 6
1.3. Gold Nanoparticle Applications 7
1.4. Valency 9
1.5. Conclusion 13
References 14

CHAPTER 2: Reactivating Resistance-Compromised Antibiotics Through Conjugation to Gold Nanoparticles 18

2.1. Introduction 18
2.2. Penicillin 19
2.3. Multivalent Display 21
2.4. Penicillin Derivatives as Multivalent Therapeutics 22
2.4.1. Our System 23
2.5. Conclusion 33
2.6. Experimental 33
References 45
Appendix 46

CHAPTER 3: Targeting Protein/Protein Interactions with Drug Coated Gold Nanoparticles: Interleukin-2/ Interleukin-2 Receptor Interaction 49

3.1. Current Problem....49
3.2. Previous Approaches and Problems....50
3.3. Hypothesis for the Disruption of Protein/Protein Interactions 52
3.4. Interleukin-2/Interleukin-2 Receptor 53
3.5. Our Method....57
3.5.1. Synthesis of Gold Nanoparticles....58
3.5.2. Synthesis and Characterization of Drug/AuNP Conjugates 59
3.5.3. Quantitation of Drugs Conjugated to the AuNP 62
3.5.3.1. Methanol Precipitation Protocol 62
3.5.3.2. Particle Decomposition Protocol 64
3.5.3.3. Overlapping Peak Absorbance's – Protocol 64
3.5.4. Demonstration that the Drug Coated AuNPs bind to IL-2 66
3.5.5. Biophysical Characterization – Biacore....68
3.5.5.1. Biacore 2000 Analysis 69
3.5.5.2. Biacore T100 Analysis with Dialed in Drugs/AuNP....78
3.6. Conclusion 87
3.7. Experimental....88
References....92
Appendix....95

LIST OF TABLES

		Page
Table 1	Properties of Small Molecule Drugs versus Gold Nanoparticles Therapeutics	9
Table 2	Comparison of Multivalent Scaffolds and Control Afforded over their Properties	12
Table 3	Summary of Synthetic Attempts to Modify from the A Region	24
Table 4	Synthetic Routes for Derivitization to the B Region	28
Table 5	Maximum Percent Growth Inhibition of MSSA and MRSA by **EAK-223** and **KDK-1022,** Both Free and Conjugated to Gold Nanoparticles (denoted NP)	30
Table 6	Drugs/particle via MeOH precipitations	63
Table 7	Dissociation Constants Based on Biacore data and Scrubber fitted	75
Table 8	2:1 Dissociation Constant Values for Analytes 4-8, and 1:1 Dissociation Constants for Analytes 1-3	77
Table 9	Initial K_d Summary	78
Table 10	Summary of the Bia Evaluation Data	84
Table 11	Summary of Final K_d	86
Table E1	Molar Feed Ratios Required to Obtain Specific Drugs/NP	90

LIST OF FIGURES

		Page
Figure 1	Photograph of Aqueous Gold Nanopheres; Color Change Observed as a Function of Size, 4 – 40 nm	2
Figure 2	Gold Based Drug Compounds; Sodium Aurothiomate (Myocrisin™), Aurothioglucose (Solganol™) and Auronofin (Ridauro™)	4
Figure 3	Number of Publications on Metal Nanoparticles over the last 19 years	4
Figure 4	Five Basic Antibiotic Scaffolds	18
Figure 5	Some Synthetically Derivatized Penicillin Compounds	20
Figure 6	Penicillin Core with 6-Aminopenicillianic Acid and Penicillin G	23
Figure 7	Thiolated Penicillin Derivatives for Conjugation to Gold Nanoparticles	29
Figure 8	Surface Rendering of an X-Ray Crystal Structure of a 15 KDa Protein and a 2.0 nm Gold Nanoparticle	53
Figure 9	Synthetic Antagonists for IL-2/IL-2R	55
Figure 10	Surface Rendering of an X-Ray Crystal Structure of Interleukin-2 with **1** bound. **1** is indicated in red	56
Figure 11	Base Compounds for IL-2/IL2R Interaction	57
Figure 12	Active IL-2 Drug with Linker and Disulfide for Nanoparticle Attachment	58
Figure 13	Transmission Electron Microscope Image of 2.0 nm para-Mercaptobenzoic Acid Protected Gold Nanoparticles with 10 nm Scale bar	59

Figure 14 Reduction of the Disulfide Bond on the Active Drug and Exchange onto the PMBA Protected Gold Nanoparticle.....60

Figure 15 Effects of Drug **4**:(PMBA) Feed Ration on 2.0 nm Particle Gel Mobility. Left to right, the Molar Feed Ratio of Drug **4**:PMBA was 0:1, 0.25:1, 0.5:1, 1:1, 2:1, 4:1, 8:1 and 16:1. Feed Ratios Higher than 8:1 were not Visualized Due to Aqueous Insolubility.....61

Figure 16 Drug/Nanoparticle Conjugates Traveling into an Acrylamide Gel and the Blank (p-MBA coated NP) In Lane 9 67

Figure 17 Drug/Nanoparticle (DNP)IL-2 Binding Visualized Non-Denaturing PAGE. Lane:1. IL-2;2. IL-2 + 8:1 Feed Ratio DNP; 3. IL-2 + 0.5:1 Feed Ratio DNP; 4. IL-2 + Glutathione-coated NP; 5. DNP from Lane 2 only; 6. DNP From Lane 3 only; 7. Glutathione-coated NP. (**A**) Gel Prior To Staining. (**B**) Coomassie Stain of (A). (**C**) An Autometallographic Stain of (A).....67

Figure 18 Number of Published Papers Utilizing Commercial Optical Biosensor in the Last 9 Years 68

Figure 19 Analyte 8 over Flow Cell 1.....70

Figure 20 Sensograms of all Analytes Injected Over all four Flow Cells.....71

Figure 21 Glutathione Coated Nanoparticles on Flow Cell 1 72

Figure 22 1:1 Binding Model of all eight Analytes.....73

Figure 23 Residuals of the 1:1 Binding Shown in Figure 22 73

Figure 24 2:1 Binding Model of All Analytes 76

Figure 25 Drugs per Nanoparticle Obtained and Corresponding Feed Ratio 79

Figure 26 Binding Isotherms for Flow Cell 2 81

Figure 27 Binding Isotherms from Flow Cell 3 82

Figure 28 Binding Isotherms from Flow Cell 4 83

Figure 29 Binding Isotherms for Active Nanoparticle Conjugates 85

Figure 30 Binding Isotherms for the Inactive Nanoparticle Conjugates 86

Figure E1 Transmission Electron Microscope (TEM) Image of 2.0 nm Gold Particles. Scale bar = 10 nm 41

Figure E2 Transmission Electron Microscope (TEM) Image of (KDK-1022)-NP. Scale bar = 20 nm 42

Figure E3 Transmission Electron Microscope (TEM) Image of (EAK-223)-NP. Scale bar = 20 nm 43

Figure A1 Absorbance Profile and Extinction Coefficient for IL-2 Inactive Compound in MeOH 96

Figure A2 Absorbance Profile and Extinction Coefficient for IL-2 Active Compound in MeOH 97

Figure A3 Absorbance Profile and Extinction Coefficient for 2.0 nm Gold Particles H_2O 98

Figure A4 The Three Integral Components of Biacore 99

Figure A5 Basics of a Sensogram 100

LIST OF SCHEMES

		Page
Scheme 1	General Synthetic Scheme for the Addition of a Thiol Linker to the A Region	24
Scheme 2	Synthetic Scheme for A Region Thiolation to Procure **KDK-1022**	27
Scheme 3	General Route for B Region Thiolation	28
Scheme 4	Synthetic Conversions for **EAK-223**	28

LIST OF ABBREVIATIONS AND TERMS

6-APA	6-aminopenicillanic acid
Å	angstrom
$AlCl_3$	Aluminum tricholoride
aq	aqueous
Au	gold
AuNP	gold Nanoparticle
avg	average
bd	broad doublet
BME	beta-mercaptoethanol
Bn	benzyl
brine	saturated aqueous sodium chloride
bs	broad singlet
ca	approximately
calcd	calculated
CCR5	chemokine receptor type 5
cm^{-1}	reciprocal centimeters
d	doublet
DCC	N,N- Dicyclohexylcarbodiimide
DCM	dichloromethane

dd	doublet of doublets
DIEA	N,N-Diisopropylethylamine
DNP	drug coated nanoparticle
DMAP	4-(dimethylamino)pyridine
DMF	N,N-dimethylformamide
DMSO	dimethyl sulfoxide
DNA	deoxyribonucleic acid
dt	doublet triplets
DTT	dithiothreitol
EDC	1-ethyl-3-(3-dimethylaminopropyl)carbodiimide hydrochloride
eq	equivalent
EtOAc	ethyl acetate
EtOH	ethanol
EtOCOCl	ethyl chloroformate
$EtOHNH_2$	ethanolamine
FC	flow cell
GE	General Electric
GSH	glutathione
h	hour(s)
H_2	hydrogen gas
H_2O	water

H_3PO_4	phosphoric acid
$HAuCl_4$	hydrogen Tetrachloroaurate
HCl	hydrochloric acid
HCTU	1H-Benzotriazolium 1-[bis(dimethylamino)methylene]-5chloro-,hexafluorophosphate (1-),3-oxide
HIV	human immunodeficiency virus
HOBt	hydroxybenzotriazole
HRMS	high resolution mass spectroscopy
Hz	hertz
K_2CO_3	potassium carbonate
KCN	potassium cyanide
Kd	dissociation constant
kDa	kilodalton
IC_{50}	inhibitory concentration: 50 %
IL-2	Interleukin-2
IL-2R	Interleukin-2 Receptor
IL-2Rα	Interleukin-2 alpha receptor
m	multiplet
M	molar
MeOH	methanol
MHB	mueller hinton broth

MHz	megahertz
MIC	minimum inhibitory concentration
min	minute(s)
mM	millimolar
MRSA	methicillin-resistant *Staphylococcus aureus*
MsCl	mesylchloride
MSSA	methicillin-susceptible *Staphylococcus aureus*
N_2	nitrogen gas
$NaBH_4$	sodium Borohydride
NaCl	sodium chloride
$NaHCO_3$	sodium bicarbonate
Na_2S	sodium sulfide
NaOH	sodium hydroxide
NHS	N-hydroxysuccinimide
nm	nanometer
NMM	n-methylmorpholine
NMR	nuclear magnetic resonance spectroscopy
NP	nanoparticle
OD	optical density
PAGE	polyacrylamide gel electrophoresis
PBPs	Penicillin binding proteins

PBP2a	Penicillin binding protein 2 alpha
Pd/C	palladium on carbon
p-MBA	para-mercaptobenzoic acid
rpm	rotations per minute
rt	room temperature
RU	responce unit
s	singlet
SDS	sodium dodecyl sulfate
SPR	surface plasmon resonance
TCEP	tris-carboxyethyl phosphine
TEM	transmission electron microscopy
TFA	trifluoroacetic acid
THF	tetrahydrofuran
TIS	triisopropylsilane
TK	tris-potassium buffer
TMS	trimethylsilane
μM	micromolar
UV	ultra-violet
V	volt

Chapter 1

Gold and Gold Nanoparticles

1.1. Gold through the Ages

Gold has been used for art, jewelry, coinage and medicine throughout the history of civilization. The extraction of gold dates back to the 5th millennium B.C. near Varna in Bulgaria. By 1200 B.C., it was being extracted by the ton in Egypt and was used in the construction of the statue of King Tut (Touthankamon).[1] The use of gold in stained glass and ceramics is the first known example of colloidal gold. Depending on the size, shape and degree of aggregation, colloidal gold can appear red, purple, and blue amongst many other colors. The Lycurgus cup from Roman times, 4th century A.D., is an example of the unique optical properties of nanoparticles; it appears green in reflected light yet red in transmitted light. Various colors reflect the plasma oscillations upon irradiation with Ultra-Violet light at various wavelengths (**Figure 1**).[2] The bulk dielectric constant for gold lies in the visible region of the electromagnetic spectrum, which is why we see such brilliant colors.[3]

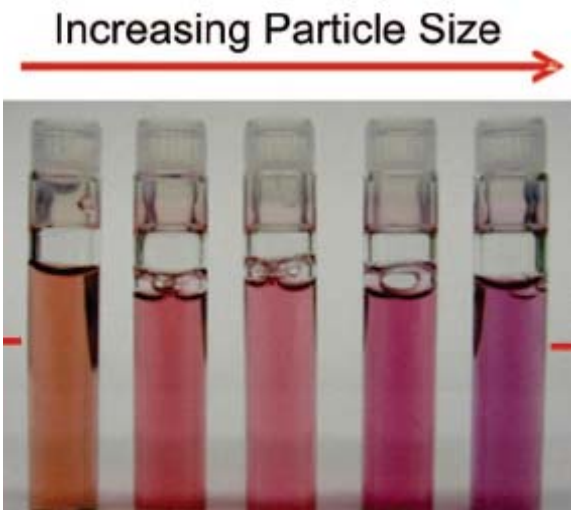

Figure 1. Photograph of Aqueous Gold Nanospheres; Color Change Observed as a Function of Size, 4 - 40 nm.[2]

In the middle ages, the exploration of the curative properties of gold had begun. Gold was utilized for the treatment of various diseases, such as venereal problems, heart disease, tumors, dysentery, epilepsy and the diagnosis of syphilis.[1] In the 17th century, Nicholas Culpepper advocated for the use of gold in treatment of fevers, depression and fainting. During the 19th century, a 'muriate of gold and soda,' a mixture of gold chloride and sodium chloride was used to treat syphilis.[4] In 1890, German scientist Robert Koch discovered that gold cyanide was bacteriostatic towards *tubercle bacillus*. Subsequently, in 1920 gold therapies were introduced to treat tuberculosis. It had been suggested that tubercle bacillus was a potential cause for rheumatoid arthritis and in turn gold was implicated in the treatments for this disease as well. Over time, gold therapy was proven fruitless for tuberculosis. However, the Empire Rheumatism Council sponsored a thirty year clinical

study which proved the effectiveness of using gold compounds to treat rheumatoid arthritis.[4] After this confirmation, gold drugs were implemented in the treatment for a variety of other rheumatic diseases, including psoriatic arthritis, juvenile arthritis, palindromic rheumatism, and discoid lupus erythematosus, not to mention the use in treating numerous inflammatory skin disorders.[4]

Rheumatoid arthritis is an autoimmune disease; progressive inflammation erodes the cartilage in the joints and leads to pain, deformity and immobility. Raised levels of cytokines, leukotrienes and prostaglandins are responsible for the progressive inflammation.[4] The gold compounds initially used to treat rheumatoid arthritis were oligomers, sodium aurothiomalate (Myocrisin™) and aurothioglucose (Solganol™); both gold (I) thiolates. Unfortunately, these compounds needed to be administered by deep intramuscular injection, this promoted rapid absorption but also caused a major side effect. Gold is rapidly cleared by the bloodstream and distributed into the kidneys, where it accumulates and causes nephrotoxicity, other side effects include occasional liver toxicity, mouth ulcers and skin reactions.[5] In 1985, auronofin (Ridauro™) was introduced as the first orally-available gold-based therapeutic (**Figure 2**).[4] The paramount and unprecedented oral administration of Ridauro™ provided several advantages, including a reduced tissue retention of gold which appreciably reduces renal toxicity. Unfortunately, the decrease in side effects is countered by a decrease in efficacy compared to the oligomeric gold (I) thiolates.

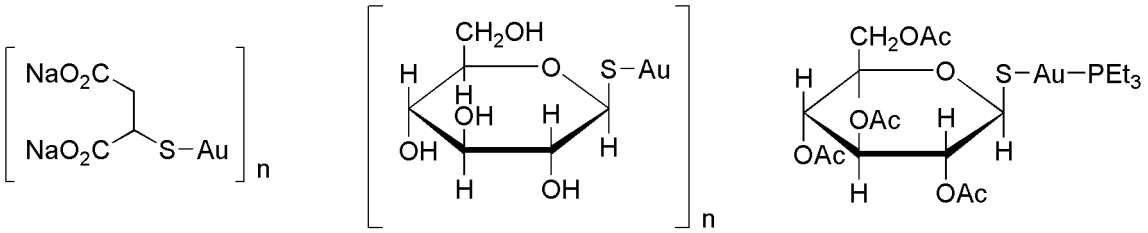

Figure 2. Gold Based Drug Compounds; Sodium Aurothiomalate (Myocrisin™), Aurothioglucose (Solganol™), and Auronofin (Ridauro™).

1.2. Metal Nanoparticles

Metal nanoparticles[6-8] are kinetically stable suspensions of nanometer-sized metals (1 nm – 200 nm). They have been synthesized from gold, silver, platinum, copper, nickel and palladium. The research devoted to metal nanoparticles has exploded over the last 15 years (**Figure 3**). This research has spanned the fields of electronics, energy development and applications in medicine.

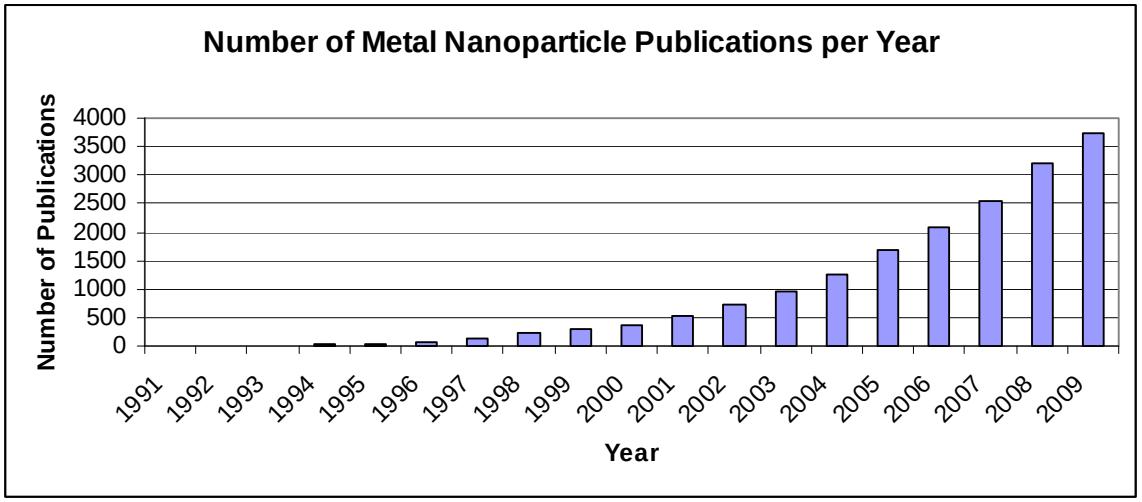

Figure 3. Number of Publications on Metal Nanoparticles over the last 19 years.

1.2.1. Synthesis

Synthesis of metal nanoparticles is typically achieved via solution-phase procedures in which a metal precursor complex is reacted with a chemical reducing agent. The first reduction of a gold salt was performed by Michael Faraday in 1857 with phosphorous in a two phase system.[9] The two most common synthetic routes to gold nanoparticles employ either trisodium citrate or $NaBH_4$ as reducing agents and $HAuCl_4$ as the metal precursor.[10-13]

1.2.1.1. Citrate Reduction of Gold Nanoparticles

The citrate reduction method yields gold particles whose diameters are determined largely by the initial citrate:$[AuCl_4]^{1-}$ stoichiometry. Turkevich in 1951 and Frens in 1973 both utilized the citrate reduction method.[2] Syntheses employing the reduction of gold salts with citrate generally yield particles with diameters ranging from 5 nm to 200 nm with <10 % size dispersity.

1.2.1.2. Brust Synthesis of Gold Nanoparticles

Research in nanotechnology skyrocketed (**Figure 3**) after Brust reported new synthetic conditions for organic-soluble gold nanoparticles in 1994.[14] The Brust synthesis of gold nanoparticles employs $NaBH_4$ in the reduction of $[AuCl_4]^{1-}$ and is typically performed in the presence of long-chain alkyl thiol ligands.[10] Thiols bind to the metal cluster early in the growth phase providing a steric barrier that prevents further growth. Particles isolated using $NaBH_4$ reduction can be tuned from 1 nm to ca. 10 nm in diameter with 10% size

dispersity. Both the citrate and $NaBH_4$ reduction syntheses require purification steps to obtain a narrow range of nanoparticle sizes. This purification can be achieved by fractionalization, ripening, etching or size chromatography. In the past few years, Murray, Tsukuda, Dass and Jin have all reported molecular formulas after purification for their gold nanoparticle conjugates.

Dr. Chris Ackerson in the Kornberg lab at Stanford, developed enhanced methods of gold nanoparticle synthesis that result in precisely defined 1.5 nm, 2.0 nm, or 3.0 nm diameter gold clusters.[15, 16] Dr. Ackerson utilized a modified single phase Brust synthesis that was successful without the need for purification. To date, this method is the only synthesis that reports a single step for making a molecule. The 2.0 nm diameter particles have a proposed empirical formula of $Au_{144}(SC_6H_4CO_2H)_{60}$.

1.2.2. Modification

A key feature of gold nanoparticles is that their surfaces may be modified with nearly any thiol-containing small molecule or polymer.[6] Moreover, using ligand place exchange reactions first described by Murray,[17] combinations of two or more chemically distinct ligands can be attached to a single nanoparticle to impart multiple functions and versatility.[11] The ability to create mixed thiol monolayers on a nanoscale platform provides a powerful tool that can be used to improve water solubility, tune sterics, and control cellular

internalization. In addition, it allows the fabrication of multivalent molecules that have a number of potential benefits and applications.

1.3. Gold Nanoparticle Applications

Gold nanoparticles have been utilized for applications in energy, electronics and medicine; we will focus on the strides in medicinal research. Great advances have been made in the design and synthesis of pharmaceutical compounds for the treatment of human disease in the past century. Diseases such as breast cancer and chronic mylogenous leukemia, once thought to be completely untreatable, are now survived by a large percentage of patients. However, it is common knowledge that the depletion of commercial drug pipelines forecasts a grim future for molecular medicine and human health. The underlying cause for the upcoming shortfall of next generation drugs resides fundamentally in the approach that is taken to conduct drug discovery and detection of disease. Medical challenges to overcome in the 21st century include the emergence of drug resistant bacteria, evolving viral strains and poorly treated diseases such as brain and lung cancer, autoimmunity and neurodegenerative disorders (Alzheimer's, Parkinson's, etc.).

Medicinal research efforts with gold nanoparticles have been directed towards drug delivery systems, catalysis, anti-infective agents, chemotherapeutics, detection and diagnostics, as well as disruption of protein/protein interactions. Gold nano-systems are attractive due to the unique properties of gold nanoparticles. The optical properties are

dependent on size and shape, as well as the lack of toxicity and ease of monolayer manipulation render gold nanoparticles as a technology worth pursuit.

Gold nanoparticles have been fabricated for use as sensors for early detection of many diseases and disorders. Alzheimer's disease and breast cancer have been targeted for essential early detection. Alzheimer's is a progressive disease in the brain that has been associated with high levels of tau protein. This devastating disease affects 26.6 million people worldwide and there is currently no cure. With early diagnosis, current drugs have a chance at prolonging the onset of symptoms such as intense irritability, memory loss, and aggression. The Ray group at Jackson State University in Mississippi has designed a monoclonal antibody coated gold nanoparticle based assay that can detect tau protein levels to 2 orders of magnitude better than previous assays.[18] This group has also fabricated a gold nanoparticle detection assay to target breast cancer.[19] Breast cancer is the most common cancer in women and the seconding leading cause of cancer deaths in women, but early detection has been vital for successful treatment and survival. Many other groups have utilized the unique properties of gold nanoparticles for detection assays and exploited their use as cell permeable multivalent systems.

Chemotherapeutics and radiation therapies have been the first line of defense in nearly all cancer treatments. One of the first chemotherapeutics was cisplatin. It is still used and effective, but the major issue with nearly all chemotherapies is cell toxicity. The Mukherjee group at the Mayo Clinic in Minnesota has fabricated gold nanoparticles with a

thiolated derivative of cisplatin. The cisplatin gold nanoparticle conjugate was subsequently tested against ovarian cancer cells and healthy cells. The results showed the cisplatin gold nanoparticle conjugate had comparable efficacy to cisplatin alone. It also showed the toxicity to healthy cells was nearly none, as opposed to the toxic nature of cisplatin alone.[20] The reduction in healthy cell toxicity is an important and exciting finding; this is one of many reasons why gold nanoparticle therapeutics could prove superior to small molecule drugs (**Table 1**).

Table 1. Properties of Small Molecule Drugs versus Gold Nanoparticle Therapeutics.

Small Molecule Drugs	**Nanoparticle Sized Drugs**
Unlimited Chemical Diversity	Large Chemical Diversity
Short Circulation Lifetimes/Fast Degradation	Long Circulation Lifetimes/Slow Degradation
Frequently Difficult to Pass Through Cell Membranes	Can be Designed to Pass Through Cell Membranes
Limited Valency (A few contacts must be VERY strong)	High Valency (Many weak contacts can provide activity)
Mode of Action Limited to Blocking the Action of an Enzyme	Could Open Up New Modes of Action

1.4. Valency

There are two distinct benefits associated with fabricating a ligand as a multivalent unit. The first is the potential for polyvalent binding (or even proximity binding), and the

second is control of local ligand concentration**.** Polyvalent binding is ubiquitous in biology.[21] The valency of a particle (protein, virus, cell, gold nanoparticle, etc.) is the number of connections it can make with another constituent. A few examples of polyvalency in biology include: (1) influenza attachment to cells via trimeric hemagglutinin association with sialic acid receptors, (2) *E. coli* attachment to epithelial cells via P-fimbrae proteins, and (3) regulation of gene expression by transcription factors.[22]

It has been proposed that biological systems exploit polyvalent interactions because they allow an organism to take advantage of an existing set of monovalent (and perhaps weak) ligands rather than evolving completely new, higher affinity monovalent ligands for every function. Indeed, polyvalent interactions can be very favorable, as seen in the binding of a trivalent oligosaccharide ligand to its asialoglycoprotein cell surface receptor occurs with a binding constant of 10^8 M^{-1}, even though the binding constant of the corresponding monovalent interaction between each distinct monosacharide and asialoglycoprotein is only 10^3 M^{-1}.[23]

Polyvalent binding is not the only advantage of displaying multiple copies of a ligand on a nanoparticle support. Attaching ligands to a gold nanoparticle in a multivalent display is an effective way to generate a high local concentration of binding ligands. The effect of a high local ligand concentration on binding equilibrium can be understood simply by considering Le Chatelier's principle. Binding equilibria between the surface-bound ligand

and the receptor may be shifted toward the formation of more ligand-receptor pairs in the presence of a high local ligand concentration.

A number of factors are applicable when considering the parameters of multivalent display. These factors are scaffold size, ligand orientation, valency, ligand density and subcellular location. An ideal multivalent scaffold for therapeutic design would allow control over each of these factors. Standard multivalent display scaffolds include low molecular weight molecules, dendrimers, liposomes, proteins, linear polymers, latex beads and gold nanoparticles. Based upon factors listed above, gold nanoparticles appear to be an ideal multivalent scaffold to explore the inhibition of protein/protein interactions. **Table 2** illustrates the potential superiority of AuNPs in comparison to the aforementioned multivalent scaffolds.

Gold nanoparticles have the potential to combine the cell permeability of a small molecule drug with the size comparability of protein therapeutics. The monolayer of a gold nanoparticle can be modified with virtually any thiolated compound, for example: known drugs, amino acids and glutathione. A mixed monolayer can increase the local concentration of a drug and increase the binding affinity to the target. These reasons combined with the ease of modification and the inertness of gold makes gold nanoparticles a very attractive drug delivery scaffold to explore.

Table 2. Comparison of Multivalent Scaffolds and Control Afforded over their Properties.

Multivalent Scaffold	Scaffold Size	Directed Ligand Orientation	Multivalency	Tunable Ligand Density	Subcellular Location
Low Molecular Weight Molecules	Molecular	Yes	Limited (Dimers, trimers typical)	No	No
Dendrimers	<15 nm	Yes	Yes	Yes	Yes
Liposomes	No	No	Yes	No	No
Proteins	<50 nm	No	Yes	Limited by accessibility of reactive amino acids	Yes
Linear Polymers	N/A	No	Yes	No	Yes
Latex Beads	>50 nm	No	Yes	Yes	No
Gold Nanoparticles	0.8 nm – 200 nm	Yes	Yes	Yes	Yes

The Rotello lab has demonstrated the benefits of a polyvalent system on a gold nanoparticle.[24-36] Modified gold nanoparticles with mercaptoamines and mercaptocarboxylic acids have demonstrated binding to proteins such as cytochrome C and chymotrypsin with high affinity through multiple electrostatic contacts.[24] Although this approach is predicted to lack the specificity necessary for biological applications due to non-specific binding (any protein that maintains surface charge will bind to these nanoparticles), the Rotello group has demonstrated that the target protein is inhibited from making protein/protein contacts once it is complexed to the nanoparticle.

1.5. Conclusion

Gold nanoparticles have been used since the 1970s for medicinal purposes. Recent advances include developments in drug delivery for the treatment of cancer from the Mukherjee group, progress in disease detection from the Mirkin and Ray groups, and successes in disrupting protein/protein interactions from the Rotello group. The benefits of using a nanoparticle scaffold include the tunability of size, the versatility of a mixed monolayer and the ease of synthesis.

Herein we have discussed the appeal and benefits to utilizing a gold nanoparticle scaffold for potential medicinal applications. We will further discuss our systems for utilizing a gold nanoparticle scaffold for combating multidrug resistance and enhancing the binding affinity of a known small molecule to a protein. At this point, gold nanoparticles are the attractive choice for a multitude of reasons. Among these, the ease of synthesis for a monodispersed product described by the Kornberg lab, simplicity of monolayer manipulation as initially reported by the Murray group, size comparability to protein targets as shown from Rotello, and lack of toxicity of the gold nanoparticle as demonstrate by Mukherjee and others.

References

1. Daniel, M.C. and D. Astruc, *Gold nanoparticles: Assembly, supramolecular chemistry, quantum-size-related properties, and applications toward biology, catalysis, and nanotechnology.* Chemical Reviews, 2004. **104**(1): p. 293-346.

2. Murphy, C.J., et al., *Gold Nanoparticles in Biology: Beyond Toxicity to Cellular Imaging.* Accounts of Chemical Research, 2008. **41**(12): p. 1721-1730.

3. El-Sayed, M.A., *Some interesting properties of metals confined in time and nanometer space of different shapes.* Accounts of Chemical Research, 2001. **34**(4): p. 257-264.

4. Fricker, S.P., *Medical Uses of Gold Compounds: Past, Present, and Future.* Gold Bulletin, 1996. **2**(29): p. 53-60.

5. Cottrill, R.V.P.a.S.M., Gold Bulletin, 1987. **20**(3).

6. Love, J., et al., *Self-assembled monolayers of thiolates on metals as a form of nanotechnology.* Chemical Reviews, 2005. **105**(4): p. 1103-1169.

7. Feldheim, D.L. and C.A. Foss, *Metal nanoparticles: synthesis, characterization, and applications*. 2002, New York: Marcel Dekker. ix, 338 p.

8. Daniel, M. and D. Astruc, *Gold nanoparticles: Assembly, supramolecular chemistry, quantum-size-related properties, and applications toward biology, catalysis, and nanotechnology.* Chemical Reviews, 2004. **104**(1): p. 293-346.

9. Faraday, M., Philos. Trans. R. Soc. London, 1857. **147**: p. 145-181.

10. Brust, M., et al., *Synthesis of Thiol-Derivatized Gold Nanoparticles in a 2-Phase Liquid-Liquid System.* Journal of the Chemical Society-Chemical Communications, 1994(7): p. 801-802.

11. Templeton, A., M. Wuelfing, and R. Murray, *Monolayer protected cluster molecules.* Accounts of Chemical Research, 2000. **33**(1): p. 27-36.

12. Grabar, K., et al., *Preparation and Characterization of Au Colloid Monolayers.* Analytical Chemistry, 1995. **67**(4): p. 735-743.

13. Freeman, R., et al., *Self-Assembled Metal Colloid Monolayers - An Approach to Sers Substrates.* Science, 1995. **267**(5204): p. 1629-1632.

14. Brust, M., et al., *Synthesis Of Thiol-Derivatized Gold Nanoparticles In A 2-Phase Liquid-Liquid System.* Journal Of The Chemical Society-Chemical Communications, 1994(7): p. 801-802.

15. Jadzinsky, P.D., et al., *Structure of a thiol monolayer-protected gold nanoparticle at 1.1 angstrom resolution.* Science, 2007. **318**(5849): p. 430-433.

16. Ackerson, C.J., et al., *Synthesis and Bioconjugation of 2 and 3 nm-Diameter Gold Nanoparticles.* Bioconjugate Chemistry. **21**(2): p. 214-218.

17. Hostetler, M.J., A.C. Templeton, and R.W. Murray, *Dynamics of place-exchange reactions on monolayer-protected gold cluster molecules.* Langmuir, 1999. **15**(11): p. 3782-3789.

18. Neely, A., et al., *Ultrasensitive and Highly Selective Detection of Alzheimer's Disease Biomarker Using Two-Photon Rayleigh Scattering Properties of Gold Nanoparticle.* Acs Nano, 2009. **3**(9): p. 2834-2840.

19. Lu, W.T., et al., *Multifunctional Oval-Shaped Gold-Nanoparticle-Based Selective Detection of Breast Cancer Cells Using Simple Colorimetric and Highly Sensitive Two-Photon Scattering Assay.* Acs Nano. **4**(3): p. 1739-1749.

20. Patra, C.R., R. Bhattacharya, and P. Mukherjee, *Fabrication and functional characterization of goldnanoconjugates for potential application in ovarian cancer.* Journal of Materials Chemistry. **20**(3): p. 547-554.

21. Whitesides, G., et al., *Meso-scale self-assembly.* Abstracts of Papers of the American Chemical Society, 1998. **215**: p. U43-U43.

22. Mammen, M., S.K. Choi, and G.M. Whitesides, *Polyvalent interactions in biological systems: Implications for design and use of multivalent ligands and inhibitors.* Angewandte Chemie-International Edition, 1998. **37**(20): p. 2755-2794.

23. Lee, Y. and R. Lee, *Carbohydrate-Protein Interactions - Basics of Glycobiology.* Accounts of Chemical Research, 1995. **28**(8): p. 321-327.

24. Bayraktar, H., et al., *Disruption of protein-protein interactions using nanoparticles: inhibition of cytochrome c peroxidase.* Chemical Communications, 2006(13): p. 1390-1392.

25. You, C., M. De, and V. Rotello, *Mono layer-protected nanoparticle-protein interactions.* Current Opinion in Chemical Biology, 2005. **9**(6): p. 639-646.

26. You, C., et al., *Tunable inhibition and denaturation of alpha-chymotrypsin with amino acid-functionalized gold nanoparticles.* Journal of the American Chemical Society, 2005. **127**(37): p. 12873-12881.

27. Verma, A. and V. Rotello, *Surface recognition of biomacromolecules using nanoparticle receptors.* Chemical Communications, 2005(3): p. 303-312.

28. Sandanaraj, B., et al., *Noncovalent modification of chymotrypsin surface using an amphiphilic polymer scaffold: Implications in modulating protein function.* Journal of the American Chemical Society, 2005. **127**(30): p. 10693-10698.

29. Arvizo, R., A. Verma, and V. Rotello, *Biomacromolecule surface recognition using nanoparticle receptors.* Supramolecular Chemistry, 2005. **17**(1-2): p. 155-161.

30. Verma, A., J. Simard, and V. Rotello, *Effect of ionic strength on the binding of alpha-chymotrypsin to nanoparticle receptors.* Langmuir, 2004. **20**(10): p. 4178-4181.

31. Hong, R., et al., *Control of protein structure and function through surface recognition by tailored nanoparticle scaffolds.* Journal of the American Chemical Society, 2004. **126**(3): p. 739-743.

32. Goodman, C. and V. Rotello, *Biomacromolecule surface recognition using nanoparticles.* Mini-Reviews in Organic Chemistry, 2004. **1**(1): p. 103-114.

33. Fischer, N., et al., *Light-induced inhibition of chymotrypsin using photocleavable monolayers on gold nanoparticles.* Chemical Communications, 2004(24): p. 2866-2867.

34. Fischer, N., et al., *Reversible "irreversible" inhibition of chymotrypsin using nanoparticle receptors.* Journal of the American Chemical Society, 2003. **125**(44): p. 13387-13391.

35. Fischer, N., et al., *Inhibition of chymotrypsin through surface binding using nanoparticle-based receptors.* Proceedings of the National Academy of Sciences of the United States of America, 2002. **99**(8): p. 5018-5023.

36. Boal, A. and V. Rotello, *Fabrication and self-optimization of multivalent receptors on nanoparticle scaffolds.* Journal of the American Chemical Society, 2000. **122**(4): p. 734-735.

Chapter 2

Reactivating Resistance-Compromised Antibiotics Through Conjugation to Gold Nanoparticles

2.1. Introduction

Infectious diseases are the second leading cause of death around the world and the third leading cause of death in economically developed countries.[1, 2] These statistics are largely due to the emergence of bacterial strains that are resistant to multiple antibiotics. Historically, antibiotics have come from just five molecular scaffolds whose life spans have been extended by generations of synthetic modification (**Figure 4**).[3] Resistance to these drugs primarily arises from three major mechanisms: target mutation, enzymatic inactivation and efflux pumps.[4] The development of therapeutics capable of withstanding these resistance mechanisms is an important and ongoing challenge to improving global health.

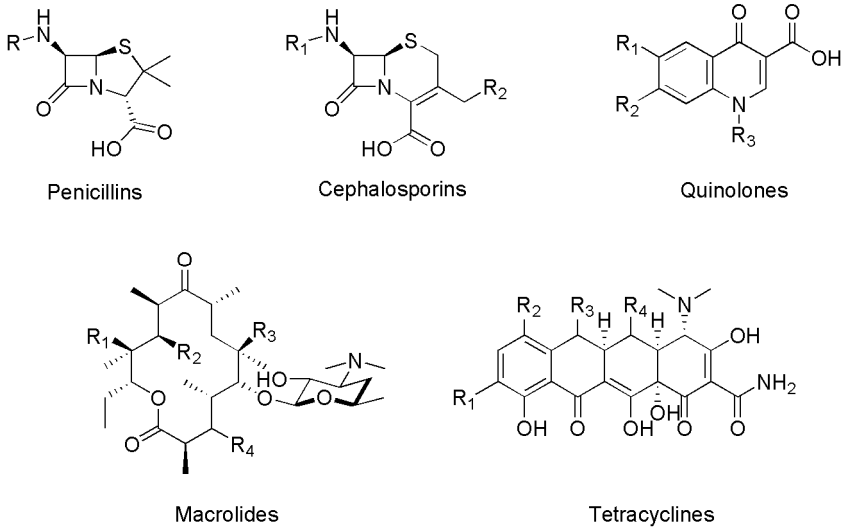

Figure 4. Five Basic Antibiotic Scaffolds.

2.2. Penicillin

First discovered accidentally by Sir Alexander Fleming, penicillin was utilized during World War II to save countless lives from bacterial infections. About a year after its massive production for use, resistant bacterial strains began to emerge. Since this time penicillin has been modified synthetically to extend its lifespan as a useful antibiotic. The extensive modifications of the penicillin scaffold include small molecules that act as both broad and narrow spectrum antibiotics, in addition to those capable of acting toward gram-negative bacterial strains. Some of the most commonly prescribed penicillin derivatives are depicted in **Figure 5**.

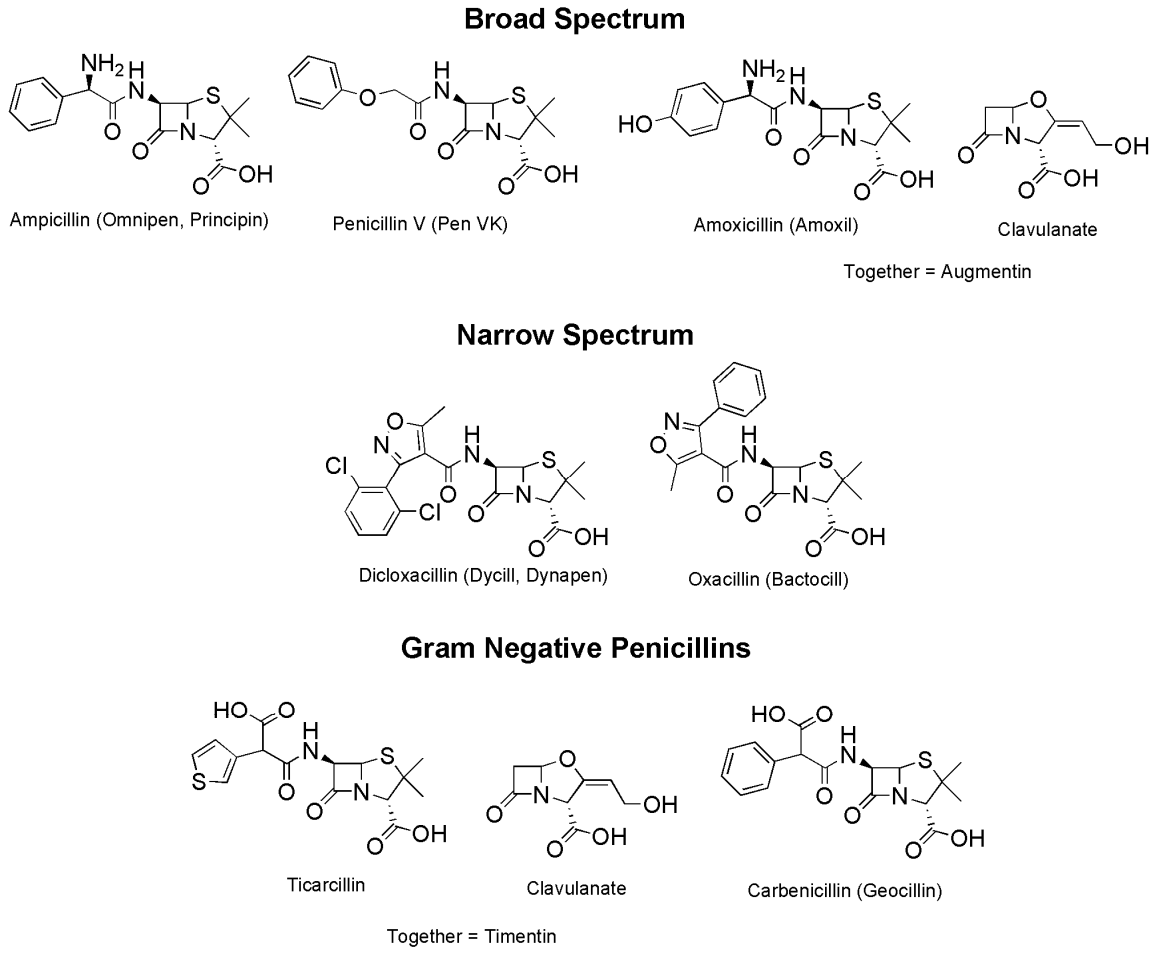

Figure 5. Some Synthetically Derivatized Penicillin Compounds.

The precedent of modifying the penicillin backbone was also employed for this scientific endeavor in order to extend the antibiotic's lifespan and efficacy. Unlike previous modifications however, our goal was to decorate penicillin with a free sulfahydryl for conjugation to gold nanoparticles. We reasoned that displaying penicillins on the surface of

gold nanoparticle might increase their efficacy through the multivalent display capable with gold nanoparticle conjugation.

2.3. Multivalent Display

Multivalency is depicted here with the display of more than one small molecule ligand on a gold nanoparticle scaffold. It could offer many advantages over traditional small molecule approaches for the treatment of infectious disease. For instance, small-molecule drugs typically function through the formation of a single high-affinity contact to a biological target. Slight alterations in this lone contact as a result of even a single target mutation can drop the binding affinity dramatically, rendering the drug ineffective. A nanoscale system equipped with multiple copies of a ligand that binds to the target would constitute a multivalent therapeutic; that may be less susceptible to resistance via target mutation. Multivalent binding enables the creation of a single high-affinity binder through the conjugation of multiple binders whose individual affinities for the target may be relatively weak. Since the strength of a multivalent binder for its target is due to the collective interactions of several binders, a pathogen mutation that removes any one contact may not result in a large enough decrease in binding affinity to prevent the desired therapeutic response. The potential benefits of multivalent nanoscale therapeutics were demonstrated recently in our labs using 2.0 nm diameter gold nanoparticles. We showed that a weak CCR5 binder and biologically inactive small molecule could be transformed into a multivalent gold

nanoparticle conjugate that effectively inhibited HIV-1 fusion to peripheral blood mononuclear cells in vitro.[5]

Our group previously demonstrated that small molecules displayed in a multivalent fashion on gold nanoparticles could dramatically increase activity toward the prevention of viral infection versus the corresponding small molecule alone. Therefore, it became of interest to determine if gold nanoparticles have the potential to obviate the drug resistance mechanisms that are presented by bacteria, including both target mutation and enzymatic inactivation. A previous attempt to address this question focused on conjugating vancomycin to the surface of gold nanoparticles; however the unmodified gold particle and the vancomycin/nanoparticle conjugate were nearly equipotent, thus conclusions about the general applicability of this approach to overcoming bacterial drug resistance were ambiguous.[5, 6]

2.4. Penicillin Derivatives as Multivalent Therapeutics

To resolve this ambiguity, we investigated whether display of penicillin derivatives on the surface of a gold nanoparticle would "reactivate" the penicillin derivative toward lactam-resistant bacteria. Penicillin was chosen as our test example because it is the archetypal example of an antibiotic that has been compromised via both target mutation and enzymatic inactivation. The mechanism of enzymatic inactivation involves lactamase enzymes, which hydrolyze the lactam ring of penicillins, rendering them incapable of binding to their target penicillin binding proteins (PBPs).[7] We posited that penicillin derivatives

conjugated to gold nanoparticles might preclude attack by lactamases due to steric and/or electronic factors. This hypothesis was based in part on results from Mirkin's lab, which showed that double stranded DNA attached covalently to gold nanoparticles is stable against nuclease degradation due to the high local salt concentration around the nanoparticle.[8] We show that conjugation of penicillin derivatives to gold nanoparticles was able to transform a resistance-compromised class of antibiotics into nanoscale conjugates with antibiotic activity.

2.4.1. Our System

The initial hypothesis was to test penicillin bound gold nanoparticles for inhibition of the growth of methicillin-susceptible and methicillin-resistant *Staphylococcus aureus* (MSSA and MRSA, respectively). We wanted to attach a thiol linker to the R position and the carboxylic acid position of the penicillin core, labeled A and B respectively in **Figure 6**, utilizing 6-aminopenicillanic acid (6-APA) and penicillin G as starting materials.

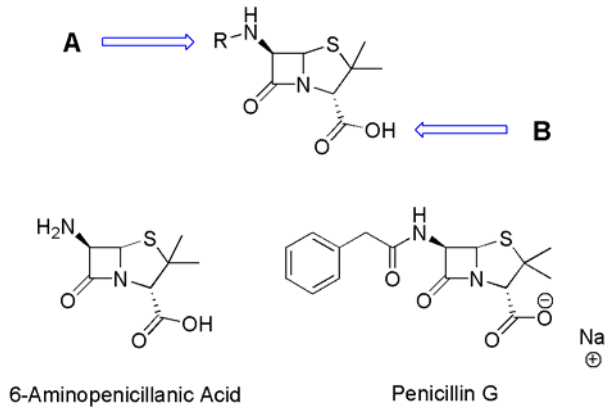

Figure 6. Penicillin Core with 6-Aminopenicillanic Acid and Penicillin G.

To this end, we attempted various protecting groups, amide coupling strategies, and deprotection conditions. Modification to the A region is generally depicted in **Scheme 1**, while **table 3** summarizes successful protecting groups, amide coupling conditions, and failed attempts at deprotection.

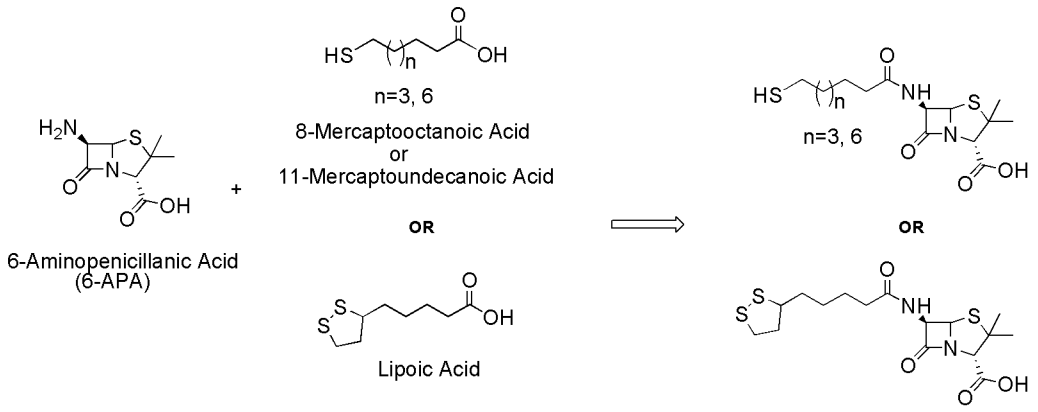

Scheme 1. General Synthetic Scheme for the Addition of a Thiol Linker to the A Region.

Table 3. Summary of Synthetic Attempts to Modify from the A Region.

Starting Materials	**Protecting Group (Carboxylic Acid on 6-APA/Thiol)**	**Coupling Conditions**	**Result**	**Deprotection Conditions**	**Result**
6-APA + 11-mercaptoundecanoic acid	No/No	DCC, HOBt, DIEA, DMF	Multiple Products		

Table 3. Continued

6-APA + 8-mercaptooctanoic acid	Yes – Benzyl/Yes-Trityl	NMM, HOBt, EDC, DMF	61% Yield	Pd/C, H_2, EtOH K_2CO_3, H_2O, THF TIS, TFA, DCM	No Reaction Multiple Products Multiple Products
6-APA + 8-mercaptooctanoic acid	Yes – Methyl/No	NMM, EDC, DMAP, DCM	39% Yield		
6-APA + 11-mercaptoundecanoic acid	Yes – Benzyl/Yes-Disulfide	NMM, HOBt, EDC, DMF	Multiple Products		
6-APA + 11-mercaptoundecanoic acid	Yes – Benzhydryl/ Yes- Disulfide	NMM, HOBt, EDC, DMF	96% Yield	TIS, TFA, DCM, 0°C	No Reaction
6-APA + 8-mercaptooctanoic acid	Yes – Benzhydryl/ Yes- Trityl	NMM, HOBt, EDC, DMF	88% Yield	Anisole, TFA, DCM, 0°C Anisole, $AlCl_3$, DCM, -50°C Formic Acid, H_2O TIS, TFA, DCM, 0°C	No Reaction No Reaction No Reaction Multiple Products

Table 3. Continued

6-APA + Lipoic Acid	Yes – 4-nitrobenzyl	NMM, HOBt, EDC, DMF	28% Yield	Pd/C (0.1eq), H_2, EtOH Pd/C (0.5eq), H_2, EtOH $Na_2S{\cdot}9H_2O$ THF, 0°C $Na_2S{\cdot}9H_2O$ Acetone, 0°C Pd/C (0.1eq), H_2, EtOH (on Parr Apparatus)	Multiple Products Multiple Products Multiple Products No Reaction No Reaction
6-APA + Lipoic Acid	Yes - Benzhydryl	NMM, HOBt, EDC, DMF	26% Yield	TFA, Phenol, 45°C Anisole, TFA, DCM	No Reaction No Reaction
6-APA + Lipoic Acid	Yes – 2-nitrobenzyl	NMM, HOBt, EDC, DMF	33% Yield	DCM, hν THF, hν	Multiple Products Multiple Products

In general, protection strategies proved successful; however numerous amide coupling conditions as well as the final deprotection steps remained problematic resulting in either: (i) minimal or no deprotection or (ii) complete hydrolysis of the lactam ring. With the use of an aqueous-labile protecting group (**Scheme 2**), and acid chloride activation we were able to obtain the A region thiolated penicillin, resulting in a partially pure **KDK-1022**.

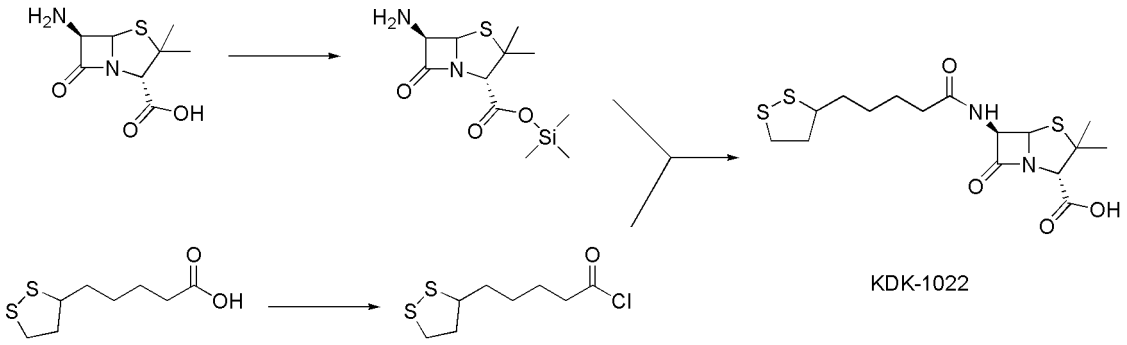

Scheme 2. Synthetic Scheme for A Region Thiolation to Procure **KDK-1022**

Test reactions for derivitization to the B region (**Scheme 3**) were initially preformed with cystamine in order to determine the most efficient coupling conditions (**Table 4**). Unfortunately none of the traditional amide bond formation conditions proved successful with a free thiol. However, we did successfully couple penicillin G with aminooctanol, followed by simple activation and partial conversion to the free thiol to give **EAK-223**, as shown in **Scheme 4**.

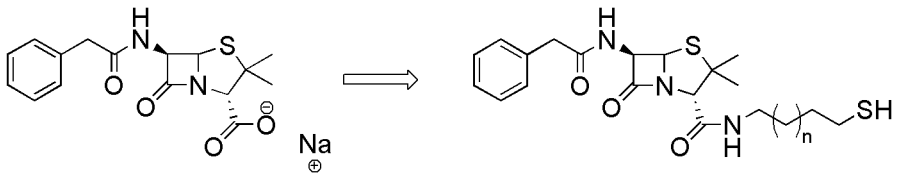

Scheme 3. General Route for B Region Thiolation.

Table 4. Synthetic Routes for Derivitization to the B Region.

Starting Materials	Coupling Conditions	Result
Penicillin G + Cystamine	NHS, DCC, 1,4-Dioxane	No Reaction
Penicillin G + Cystamine	EtOCOCl, DMF	No Reaction
Penicillin G + Cystamine	HCTU, DIEA, DMF	No Reaction
Penicillin G + Cystamine	DCC, HOBt, DMF	No Reaction
Penicillin G + Cystamine	NMM, HOBt, EDC	No Reaction
Penicillin G + Cystamine	EDC, NHS, DMF	No Reaction
Penicillin G + 8-aminooctanol	NMM, HOBt, EDC	50% Yield

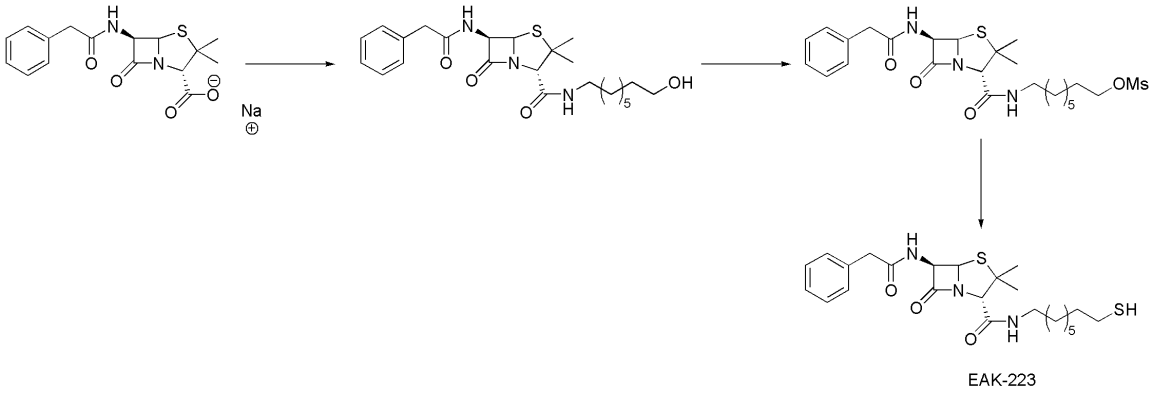

Scheme 4. Synthetic Conversions for **EAK-223.**

Once penicillin derivatives **EAK-223** and **KDK-1022** (**Figure 7**) were synthesized for subsequent thiol-mediated assembly on gold nanoparticles, we began testing the ability of a small molecule-coated gold nanoparticle to overcome antibiotic drug resistance. The base scaffold employed for **EAK-223** and **KDK-1022** conjugation were para-Mercaptobenzoic acid (pMBA)-coated gold nanoparticles with a core diameter of 2.0 nm and a proposed empirical formula of $[Au_{144}(SC_6H_4COOH)_{60}]$.[9] To improve aqueous solubility of the resultant nanoparticle conjugates, a portion of the pMBA monolayer was replaced with glutathione. Partially pure **EAK-223** and **KDK-1022** were subsequently exchanged onto the gold nanoparticles. Particle size following the ligand exchange procedure was confirmed by transmission electron microscopy and UV-visible spectroscopy.

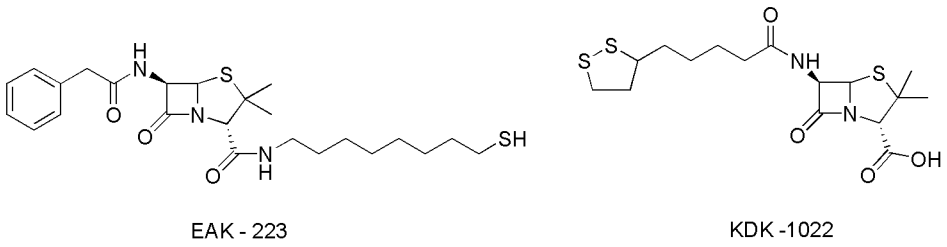

Figure 7. Thiolated Penicillin Derivatives for Conjugation to Gold Nanoparticles.

Nanoparticle conjugates were screened for activity towards growth inhibition of methicillin-susceptible and methicillin-resistant *Staphylococcus aureus* (MSSA and MRSA, respectively). Free **EAK-223,** free **KDK-1022,** and glutathione-coated nanoparticles were

screened as controls. Assays were conducted under standard broth dilution procedures[10] followed by colony counting (**Table 5**).

Table 5. Maximum percent growth inhibition of MSSA and MRSA by **EAK-223** and **KDK-1022**, both free and conjugated to gold nanoparticles (denoted NP). See text for averages and standard deviations.

	MSSA (29213)		MRSA (BAA-44)	
	Conc. μM	Inhibition %	Conc. μM	Inhibition %
KDK-1022	74	99	1400	99
KDK-1022 NP	25	99	25	99
EAK-223	210	99	420[a]	40
EAK-223 NP	25	96	25	95
Glutathione NP	25	68	25	52

[a]Solubility limit in 10% DMSO/90% H_2O. NP concentrations are the gold nanoparticle concentration.

To evaluate the efficacy of our nanoparticle conjugates, we first determined the concentration of **KDK-1022** and **EAK-223** that inhibited growth of MSSA and MRSA by 99% (**Table 5**). Free **KDK-1022** showed 99% growth inhibition of MSSA at 74 μM. However its activity towards MRSA was clearly compromised, as it did not achieve 99% growth inhibition until a concentration of 1.4 mM. Free **EAK-223** was less active against MSSA compared to free **KDK-1022**, showing 99% growth inhibition at 210 μM. This was expected because the carboxyl of penicillin is known to be important for PBP binding.[11] The activity of free **EAK-223** toward MRSA was also severely compromised as it only achieved 40% growth inhibition at 420 μM (solubility limit). Despite the drastic difference in growth

inhibition activity of our free penicillin derivatives against the two *S. aureus* strains, we observed that conjugation of these derivatives to gold nanoparticles resulted in small molecule/nanoparticle conjugates that were equipotent to both MRSA and MSSA. For example, **KDK-1022** conjugated to gold nanoparticles showed up to 99% growth inhibition of MSSA (avg. of 96% ± 3%) and up to 99% growth inhibition of MRSA (avg. of 98% ± 1%) at nanoparticle concentrations of 25 μM. **EAK-223** conjugated to gold nanoparticles was less active than **KDK-1022**/gold conjugates against both MSSA and MRSA (94% ± 3% and 94% ± 1%, respectively). However, as with **KDK-1022** conjugated to gold nanoparticles, the activity of **EAK-223**/gold conjugates did not decrease for MRSA compared to MSSA. Finally, the activity of glutathione-coated gold nanoparticles towards the growth inhibition of both MSSA and MRSA was minimal (68% and 52% respectively).

The data in **Table 5** reveal that both **EAK-223** and **KDK-1022** conjugated to gold nanoparticles showed no decrease in activity for growth inhibition of the lactam-resistant MRSA strain versus the lactam-susceptible MSSA strain. However, free **KDK-1022** and **EAK-223** showed a marked decrease in activity towards MRSA compared to MSSA. Based upon the **KDK-1022** concentrations required to achieve 99% growth inhibition of MRSA, **KDK-1022** is 14X more active when conjugated to gold nanoparticles versus free in solution. Thus, when conjugated to gold nanoparticles, these lactam derivatives appear to be less susceptible to the resistance mechanisms that render the free molecules less effective.

Penicillin resistance in MRSA is conferred by expression of the altered PBP enzyme PBP2a and lactamase. Expression of these enzymes is regulated by membrane-bound signal

transducers.[12] The activities of **KDK-1022** and **EAK-223** toward MRSA growth inhibition when conjugated to gold nanoparticles suggest that, relative to free **KDK-1022** and **EAK-223,** the conjugates either (i) bind with higher affinity to PBP2a, (ii) are less susceptible to hydrolysis by lactamase, or (iii) bind less tightly to the signal transducer proteins or otherwise interfere with the signal cascade so that PBP2a and lactamase expression cannot be upregulated. To determine which mechanism might be operating, PBP2a and lactamase expression was stimulated by culturing MRSA in broth containing 62.5 μM penicillin G. This concentration was chosen because it inhibited MSSA but not MRSA growth, suggesting lactamase and PBP2a expression in the MRSA strain. **KDK-1022**-modified gold nanoparticles were then added at 25 μM and a colony count assay performed. Under these conditions the activity of the gold nanoparticle conjugates toward MRSA growth inhibition was similar to that of MRSA cultured in the absence of penicillin G. Similar results were obtained for **EAK-223** conjugates. This suggests that **KDK-1022** and **EAK-223** modified gold nanoparticles are able to bind to PBP2a while avoiding attack by lactamase.

The importance of multivalency was also examined by decreasing the average number of **KDK-1022** ligands per particle; which was achieved by decreasing the molar ratio of **KDK-1022** utilized in the exchange. This proved to decrease the activity toward MRSA growth inhibition to 94%. The result suggests that nanoparticle binding to the penicillin binding protein may be enhanced through multivalent interactions.

2.5. Conclusion

In conclusion, it was demonstrated that conjugation of thiolated penicillin derivatives to 2.0 nm diameter gold nanoparticles produces penicillin/nanoparticle conjugates that are equipotent against both MSSA and MRSA. These results may have implications in the development of novel antibiotics, as our results indicate that resistance-compromised antibiotics may be reactivated via proper design and conjugation to gold nanoparticles. Further investigation is needed to optimize the linker composition and lengths as well as exploring the use of mixed thiol monolayers to improve the overall efficacy of these penicillin/nanoparticle conjugates.

2.6. Experimental

All ^{1}H NMR and ^{13}C NMR spectra were recorded at 25.0 ºC on a Varian Mercury spectrometer. Chemical shifts are reported in parts per million relative to DMSO-d_6 (δ 2.50) for ^{1}H NMR and relative to DMSO-d_6 (δ 39.51) for ^{13} C NMR with TMS as an internal standard, coupling constants (*J*) are in hertz (Hz). Abbreviations used are s = singlet, bs = broad singlet, d = doublet, t = triplet, and m = multiplet. FAB-MS spectra were measured via high-resolution fast atom bombardment using a matrix of nitrobenzyl alcohol. Silica gel (40 μm average particle size) was used for column chromatography. All other reagents were used as purchased (Sigma-Aldrich) unless otherwise noted.

Synthesis of EAK-223

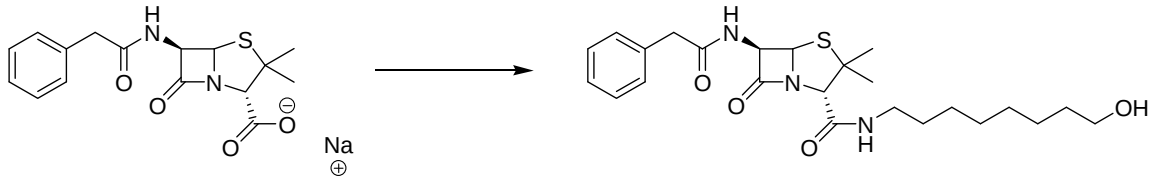

1 2

(2S,6R)-N-(8-hydroxyoctyl)-3,3-dimethyl-7-oxo-6-(2-phenylacetamido)-4-thia-1-aza-bicyclo[3.2.0]heptane-2-carboxamide (2). Benzylpenicillin sodium salt (**1**) (1.96 g, 5.51 mmol) and 8-amino-1-octanol (0.800 g, 5.51 mmol) were suspended in dry DMF (40 ml) and cooled to 0°C. To this solution was added n-methylmorpholine (NMM) (0.726 ml, 6.61 mmol), hydroxybenzotriazole (HOBT) (1.04 g, 7.71 mmol), and 1-ethyl-3-(3-dimethylaminopropyl) carbodiimide) (EDC) (1.26 g, 6.61 mmol). The solution was allowed to warm to ambient temperature overnight and then the solvent was removed under reduced pressure. The resulting viscous liquid was taken up in ethyl acetate (50 ml), and was successively washed with aqueous 10% citric acid solution, H_2O, saturated $NaHCO_3$, H_2O, and brine (50 ml each). The organic layer was then dried over anhydrous Na_2SO_4, filtered, and concentrated under reduced pressure. Flash column chromatography (0-7% MeOH/DCM gradient) of the material gave (2S,6R)-N-(8-hydroxyoctyl)-3,3-dimethyl-7-oxo-6-(2-phenylacetamido)-4-thia-1-aza-bicyclo[3.2.0]heptane-2-carboxamide (1.258 g, 50%) as a light yellow powder. ^{1}H NMR (400 MHz, DMSO-d_6) δ 8.94 (d, 1H, *J* 7.5 Hz), 8.14 (m, 1H), 7.27 (m, 5H), 5.44 (m, 2H), 4.33 (m, 1H), 4.11 (s, 1H), 3.53 (m, 2H), 3.05 (m, 2H), 1.59 (bs, 3H), 1.38 (bs, 3H), 1.24 (m, 12H); ^{13}C NMR (100 MHz, DMSO-d_6) δ 174.93, 171.12,

167.28, 136.54, 129.74, 128.89, 127.15, 71.50, 67.84, 64.80, 61.39, 58.84, 42.07, 41.22, 40.83, 33.20, 30.86, 29.55, 29.40, 27.11, 27.02, 26.12 ppm; HRMS (ESI) m/z, ($[M + H]^+$, $C_{24}H_{35}N_3O_4S$): calcd. 461.617, found 462.625.

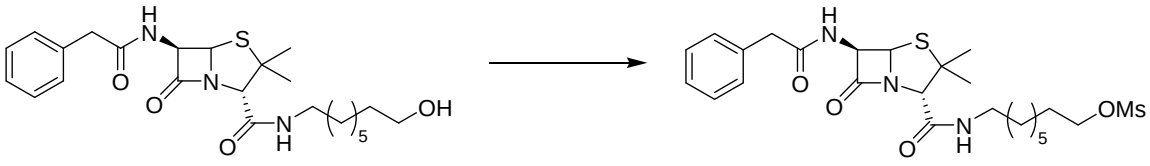

2 3

8-((2S,6R)-3,3-dimethyl-7-oxo-6-(2-phenylacetamido)-4-thia-1-aza-bicyclo[3.2.0]heptane-2-carboxamido)octyl methanesulfonate (3). (2S,6R)-N-(8-hydroxyoctyl)-3,3-dimethyl-7-oxo-6-(2-phenylacetamido)-4-thia-1-aza-bicyclo[3.2.0]heptane-2-carboxamide (**2**) (1.25 g, 2.73 mmol) was dissolved in dry dichloromethane (DCM; 25 ml) and cooled to 0°C. To this solution was added Et_3N (0.760 ml, 5.45 mmol) and MsCl (0.318 ml, 4.08 mmol). The solution was allowed to stir at 0°C, under N_2 atmosphere for 2 hrs. Then the solution was poured over ice water (25 ml), transferred to a separatory funnel and extracted with DCM (15 ml x3). The combined organic extracts were dried with Na_2SO_4, filtered, and concentrated under reduced pressure. The crude material was used in the next step without purification.

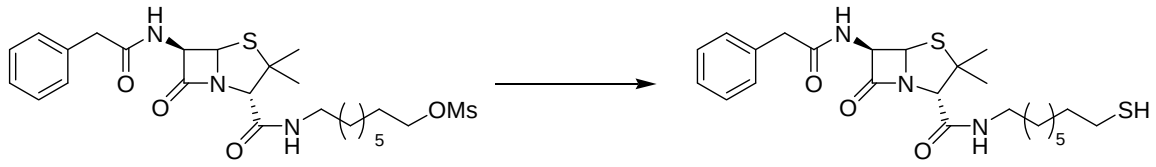

3 EAK-223

(2S,6R)-N-(8-mercaptooctyl)-3,3-dimethyl-7-oxo-6-(2-phenylacetamido)-4-thia-1-aza-bicyclo[3.2.0]heptane-2-carboxamide (EAK-223). NaSH (0.2 g, 3.5 mmol) was suspended in THF (20 ml) under N_2 atmosphere and sonicated. Then 8-((2S,6R)-3,3-dimethyl-7-oxo-6-(2-phenylacetamido)-4-thia-1-aza-bicyclo[3.2.0]heptane-2-carboxamido)octyl methanesulfonate (**3**) (1.4 g, 2.7 mmol) in THF (10 ml) was added and allowed to stir, under N_2 overnight at ambient temperature. The reaction was diluted with H_2O (30 ml) and washed with ethyl acetate (30 ml x3), and brine. The organic phase was dried with Na_2SO_4, filtered, and concentrated under reduced pressure, giving partially pure EAK-223 (1.298 g, 98%) as a light yellow powder.

Synthesis of KDK-1022

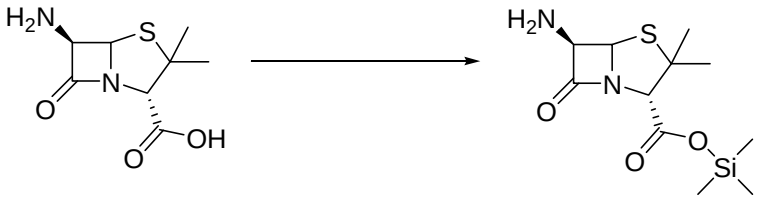

5 6

(2S,6R)-trimethylsilyl6-amino-3,3-dimethyl-7-oxo-4-thia-1-aza-bicyclo[3.2.0]heptane-2-carboxylate (6). 6-Aminopenicillanic acid (**5**) (0.600 g, 2.77 mmol) was suspended in dry DCM (30 ml). To this solution was added N,O-bis(trimethylsilyl) acetamide (0.747 ml, 3.05 mmol). The solution was allowed to run under N_2 atmosphere at ambient temperature overnight. The crude reaction mixture was used as it was in the next step without purification.

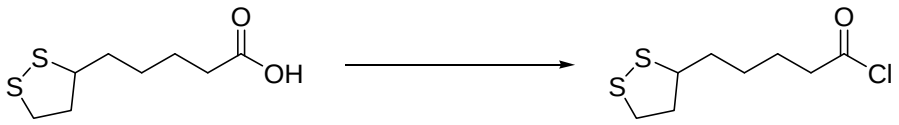

7 8

5-(1,2-dithiolan-3-yl)pentanoyl chloride (8). Lipoic Acid (**7**) (0.688 g, 3.33 mmol) was dissolved in dry DCM (15 ml) and cooled to 0^{o}C. To this solution DMF (4-5 drops) was added and oxalyl chloride (2.38 ml, 27.3 mmol). Gas evolution was observed, once bubbling stopped the solution was allowed to stir for an additional 20-30 minutes, under argon stream. Then DCM (10 ml) was added to the solution. The whole mixture was concentrated under reduced pressure. This was repeated an additional three times. Then the residue was further dried under high vacuum at ambient temperature. The crude was used in the next step without further purification.

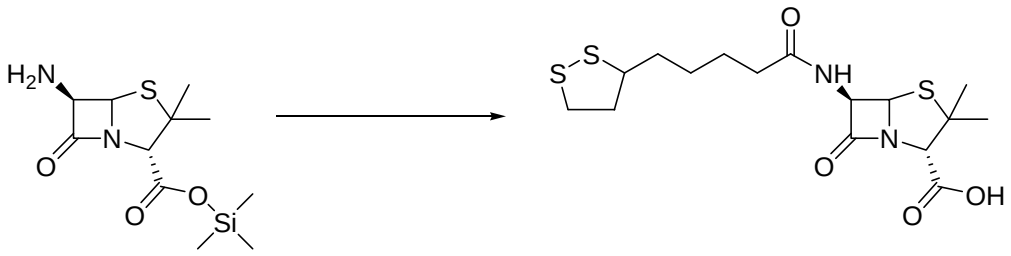

6 KDK-1022

(2S,6R)-6-(5-(1,2-dithiolan-3-yl)pentanamido)-3,3-dimethyl-7-oxo-4-thia-1-aza-bicyclo[3.2.0]heptane-2-carboxylic acid (KDK-1022). To freshly prepared (2S,6R)-trimethylsilyl 6-amino-3,3-dimethyl-7-oxo-4-thia-1-aza-bicyclo[3.2.0]heptane-2-carboxylate (**6**) (2.77 mmol) in DCM (30 ml), TEA (0.58 ml, 4.16 mmol) was added dropwise and cooled to 0^{o}C under N_2 atmosphere. 5-(1,2-dithiolan-3-yl)pentanoyl chloride (**8**) (3.30 mmol) was redissolved in DCM (5 ml) and added dropwise to (**6**). The solution was allowed to warm to ambient temperature overnight. Then the reaction mixture was diluted with EtOAc (20 ml) and aqueous 1N HCl was added to adjust pH to 2. The precipitate was filtered and rinsed with ethyl acetate. The combined organic layers were washed with 1N HCl and brine (50 ml each), dried with Na_2SO_4, filtered, and concentrated under reduced pressure. Giving partially pure KDK-1022 (0.247 g, 27%) as a reddish brown powder.

Preparation of 2.0 nm gold particles

A concentrated gold-thiol polymer stock solution composed of 1 mM $HAuCl_4$, 3.4 mM 4-mercaptobenzoic acid, and 50% aqueous methanol was adjusted to pH ~13 using sodium hydroxide. This solution was allowed to stir overnight at ambient temperature in a

sealed vessel. The solution was subsequently diluted to a final Au(III) concentration of 10 μM with the addition of methanol and water. Sodium borohydride (10 mM, aqueous) was added in a 3:1 molar ratio and after 16 hours of reaction time methanol was added to the reaction to precipitate the product. The product was collected by filtration, dissolved in water and then precipitated with methanol to obtain 2.0 nm gold particles.

Preparation of (GSH-NP)

2.0 nm gold particles (200 μM, 1.8 μmol) in H_2O and glutathione (GSH) (20 mM, 414 μmol) in 100 mM Tris-HCl were combined, and allowed to react at ambient temperature on a shaker rotisserie for 3 days. The product was precipitated and washed with methanol (3x) and collected by centrifugation at 6000 *g* to obtain GSH-NP. The GSH-NP was then re-suspended in 50% aqueous glycerol.

Preparation of (KDK-1022)-NP) and (EAK-223)-NP

GSH-NP (400 μM, 80 nmol) in H_2O and **KDK-1022** (100 mM, 8.64 μmol) in MeOH were combined and 114 μL of MeOH/H_2O/glycerol (75:12.5:12.5) was added. After 10 days, the supernatant was removed and the product was washed with methanol (3x) to remove excess **KDK-1022** and displaced GSH to obtain **(KDK-1022)-NP**. **(EAK-223)-NP** was prepared as described above.

Transmission electron microscopy

A 5 μL solution of 2.0 nm gold particles, **(KDK-1022)-NP**, and **(EAK-223)-NP** respectively were dispensed onto three separate 400 mesh carbon coated copper TEM grid (Electron Microscopy Sciences). The NP samples were allowed to incubate on the grid for 1 minute and then side-blotted with a Kimwipe. Then the grid was washed with 5 μL of milli-q treated H_2O, and side blotted with a Kimwipe. The grids were examined in a FEI CM100 microscope, operating at 100 kV accelerating voltage.

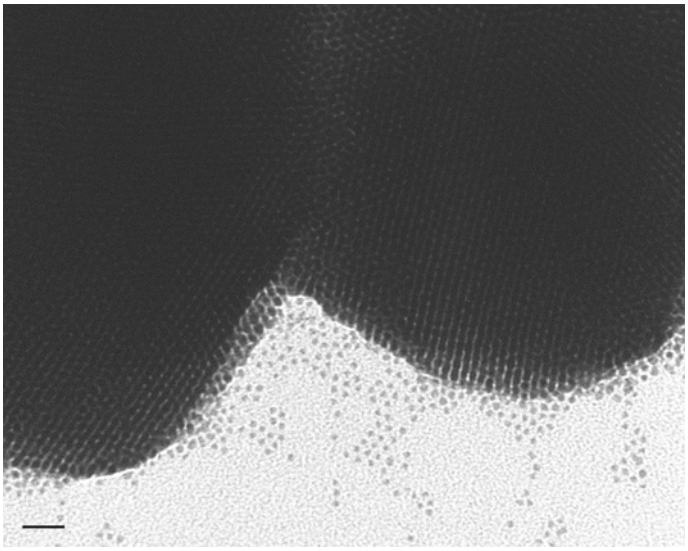

Figure E1. Transmission Electron Microscope (TEM) image of 2.0 nm gold particles. Scale bar = 10 nm.

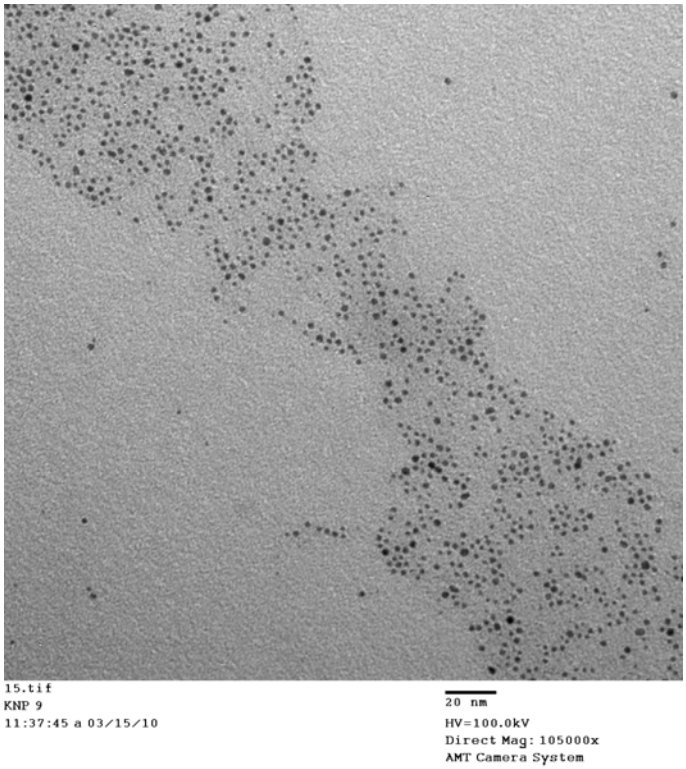

Figure E2. Transmission Electron Microscope (TEM) image of (KDK-1022)-NP. Scale bar = 20 nm.

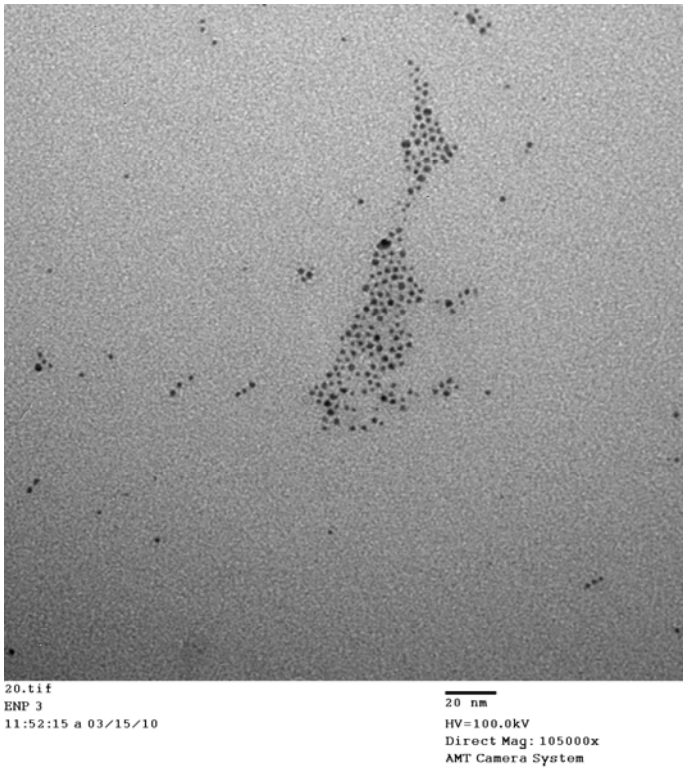

Figure E3. Transmission Electron Microscope (TEM) image of (EAK-223)-NP. Scale bar = 20 nm.

Bacterial Assays

All bacterial growth (MSSA and MRSA) inhibition assays were done in Mueller-Hinton Broth for 6 to 7 hours at 37 ºC until an OD of 0.6 was reached at 600 nm. The bacteria was then diluted to an OD of 0.002 and used as a standard and incubated with samples in a shaking incubator (225 rpm, at 37 ºC) for 16 to 20 hours. After this time samples were diluted and plated onto MHB-Agar, and MHB-Agar supplemented with

sheep's blood. The plates were then incubated at 37 ºC for 18 - 24 hours. The resultant colonies were then quantified for growth inhibition.

References

1. Morens, D.M., G.K. Folkers, and A.S. Fauci, *Emerging infections: a perpetual challenge.* Lancet Infectious Diseases, 2008. **8**(11): p. 710-719.

2. Nathan, C., *Antibiotics at the crossroads.* Nature, 2004. **431**(7011): p. 899-902.

3. Fischbach, M.A. and C.T. Walsh, *Antibiotics for Emerging Pathogens.* Science, 2009. **325**(5944): p. 1089-1093.

4. Croft, A.C., A.V. D'Antoni, and S.L. Terzulli, *Update on the antibacterial resistance crisis.* Medical Science Monitor, 2007. **13**(6): p. RA103-RA118.

5. Bowman, M.C., et al., *Inhibition of HIV fusion with multivalent gold nanoparticles.* Journal Of The American Chemical Society, 2008. **130**(22): p. 6896-+.

6. Gu, H.W., et al., *Presenting vancomycin on nanoparticles to enhance antimicrobial activities.* Nano Letters, 2003. **3**(9): p. 1261-1263.

7. Chambers, H.F., *Solving staphylococcal resistance to beta-lactams.* Trends In Microbiology, 2003. **11**(4): p. 145-148.

8. Seferos, D.S., et al., *Polyvalent DNA Nanoparticle Conjugates Stabilize Nucleic Acids.* Nano Letters, 2009. **9**(1): p. 308-311.

9. Ackerson, C.J., et al., *Synthesis and Bioconjugation of 2 and 3 nm-Diameter Gold Nanoparticles.* Bioconjugate Chemistry. **21**(2): p. 214-218.

10. CLSI, *Methods for Dilution Antimicrobial Susceptibility Tests for Bacteria That Grow Aerobically; Approved Standard - Eighth Edition.* CLSI document M07-A8, 2009. **29**(2).

11. Dalhoff, A., T. Nasu, and K. Okamoto, *Beta-lactamase stability of faropenem.* Chemotherapy, 2003. **49**(5): p. 229-236.

12. Zhang, H.Z., et al., *A proteolytic transmembrane signaling pathway and resistance to beta-lactams in staphylococci.* Science, 2001. **291**(5510): p. 1962-1965.

Appendix

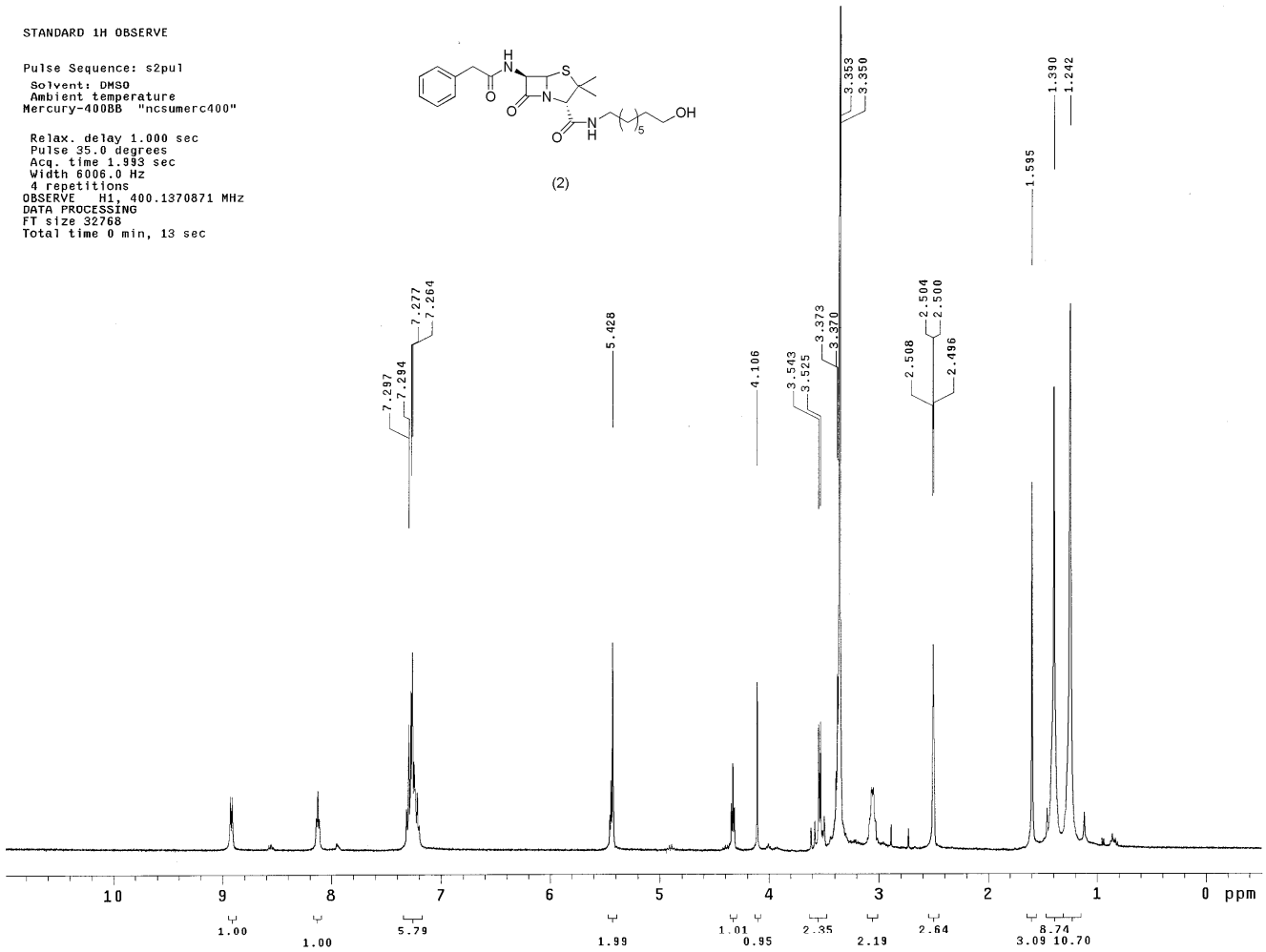
STANDARD 1H OBSERVE
Pulse Sequence: s2pul
Solvent: DMSO
Ambient temperature
Mercury-400BB "ncsumerc400"
Relax. delay 1.000 sec
Pulse 35.0 degrees
Acq. time 1.993 sec
Width 6006.0 Hz
4 repetitions
OBSERVE H1, 400.1370871 MHz
DATA PROCESSING
FT size 32768
Total time 0 min, 13 sec
(2)
7.297
7.294
7.277
7.264
5.428
4.106
3.543
3.525
3.373
3.370
3.353
3.350
2.508
2.504
2.500
2.496
1.595
1.390
1.242
10
9
8
7
6
5
4
3
2
1
0 ppm
1.00
1.00
5.79
1.99
1.01
0.95
2.35
2.19
2.64
8.74
3.09 10.70

13C OBSERVE

Pulse Sequence: s2pul
Solvent: DMSO
Ambient temperature
Mercury-400BB "ncsumerc400"

Pulse 81.2 degrees
Acq. time 1.199 sec
Width 28011.2 Hz
28544 repetitions
OBSERVE C13, 100.6145284 MHz
DECOUPLE H1, 400.1330648 MHz
Power 44 dB
continuously on
WALTZ-16 modulated
DATA PROCESSING
Line broadening 1.0 Hz
FT size 131072
Total time 14 hr, 30 min, 47 sec

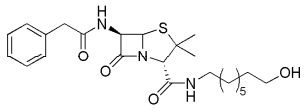

(2)

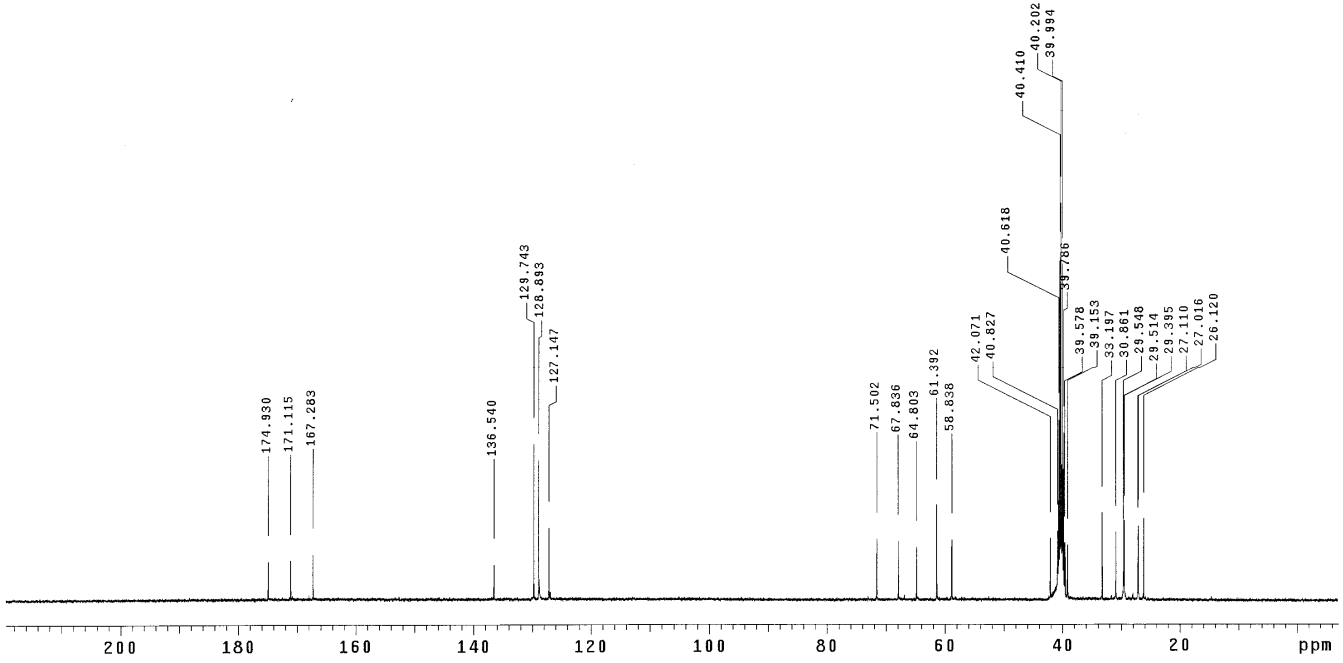

Chapter 3

Targeting Protein/Protein Interactions with Drug Coated Gold Nanoparticles: Interleukin-2/Interleukin-2 Receptor Interaction

3.1. Current Problem

Current medicinal chemistry protocols rely on targeting an aberrant protein via a one drug: one protein design paradigm. This approach is underpinned by the ability to control protein function by designing a drug to bind to a discrete pocket in the target protein. Once the drug is bound, the drug exerts artificial control of protein function eliciting a therapeutic response. This approach works well for certain classes of proteins (such as enzymes), and to date, approximately 500 proteins have been targeted successfully by this approach.[1]

Although recent successes are promising, one must recognize that at any given moment, the human body contains upwards of 10,000,000 distinct proteins.[2] Thus, we are forced to draw the sobering conclusion that only ~0.0005% of all human proteins have been successfully targeted for disease intervention. The paucity of proteins that have been targeted successfully for therapeutic intervention is due to the fact that most proteins exert their biological functions by interacting with other proteins. Proteins do not function in general as single entities, but as precisely positioned aggregates with two or more other proteins. The ability to design agents that disrupt specific protein/protein interactions would allow virtually every protein to be utilized as a therapeutic target and would represent a new paradigm in medicinal chemistry.

3.2. Previous Approaches and Problems

The disruption of a protein/protein interaction is conceptually straightforward;[3] however it can be a difficult challenge for drug discovery efforts. Protein surface areas are large and have multiple points of contact with a protein receptor. An ideal drug for disrupting protein/protein interactions must possess:

1. A high affinity for the surface of the protein target.
2. Comparable size to the protein target.
3. Cell permeability.
4. Non-immunogenicity.

There are many approaches to targeting the disruption of protein/protein interactions such as monoclonal antibodies, small molecules and mixed monolayer protected nanoparticles. However, these approaches are limited by the following six pitfalls according to Yin and Hamilton.[3] First, the key protein residues involved in binding are often unclear therefore, mimicking small molecules after natural ligands can be difficult. Second, the protein/protein interfaces can be very large, typically about 1600 $Å^2$ whereas a typical small molecule drug only covers about 100 $Å^2$. Third, the complexity of the binding regions of proteins is often noncontiguous, making it impossible to mimic with simple synthetic peptides. Fourth, many protein/protein interfaces are similar which makes targeting a specific protein difficult. Fifth, libraries of small drug-like molecules have been synthesized

for the disruption of protein/protein interactions however, thus far few have proven to be useful after screening. And sixth, it can be extremely challenging to monitor binding directly and the studies required to determine a potential target can be tedious.[3] Over the last few years, developments have been made in bioinformatics which provide useful insight into determining hot spots of protein/protein interactions that provide potential sites for small molecule-mediated disruption. These insights have led to more informative clues for drug design, making library screening still tedious but more specific.

Small molecule therapies for targeting the complexities of a protein surface is difficult, but there have been some successes in targeting surface exposed histidines with transition metal complexes[4] and cyclodextrin dimers.[5] However when dealing with the complicated topological features of protein surfaces (numerous hydrogen bonding, hydrophobic and electrostatic interactions) it is advantageous to explore large surface scaffolds that are more size comparable to the target itself.

The Rotello group at the University of Massachusetts, was able to successfully target α-chymotrypsin with amino acid functionalized gold nanoparticles.[6] Another approach to disrupting protein/protein interactions is the use of protein therapeutics. Protein-based therapeutics can recognize a protein surface with high affinity (through multivalent binding), and due to their comparable size, disrupt their targeted protein/protein interaction efficiently. Dr. Burgess at Texas A & M University was able to use solid phase synthesis to mimic proteins and disrupt the interaction of the nerve growth factor and its transmembrane tyrosine kinase receptor.[7] However, protein therapeutics are typically not cell permeable, are

frequently immunogenic, and are inconvenient to administer (they must be injected). To date, there is a limited number of protein-based therapeutics on the market that inhibit protein/protein interactions efficiently (e.g. Enbrel or Remicade to control autoimmunity).

3.3. Our Hypothesis for the Disruption of Protein/Protein Interactions

Based upon the aforementioned considerations, we posited that gold nanoparticles represent ideal platforms for therapeutic development toward inhibiting protein/protein interactions; based upon the size, shape, and ease with which gold nanoparticle surfaces may be chemically modified, as well as their demonstrated inertness in cells and live animals.[8-15] Due to the multivalent character[10] of drug-coated nanoparticles, we can augment the affinity of a given drug to its protein target. Even if the individual drug binds a desired protein target weakly, when attached to a nanoparticle, its multivalent character will collectively endow the drug-coated nanoparticle with enhanced binding properties and transform the drug into a strong binder. Increasing the available surface area of the therapeutic will improve its ability to inhibit two proteins interacting via large surface area contacts (sterics). Specifically, the total footprint of the nanoparticle will be large enough to disrupt all contact points between the protein targets (**Figure 8**). This approach is potentially applicable to disrupting any protein/protein interaction because the overall strategy of drug-coated nanoparticles combines the cell permeability of synthetic organic drugs with the size and multivalency of protein therapeutics. In order to validate our hypothesis, we have chosen to investigate the

nanoparticle-mediated disruption of the well-characterized Interleukin-2/Interleukin-2 Receptor (IL-2/IL-2R) interaction.

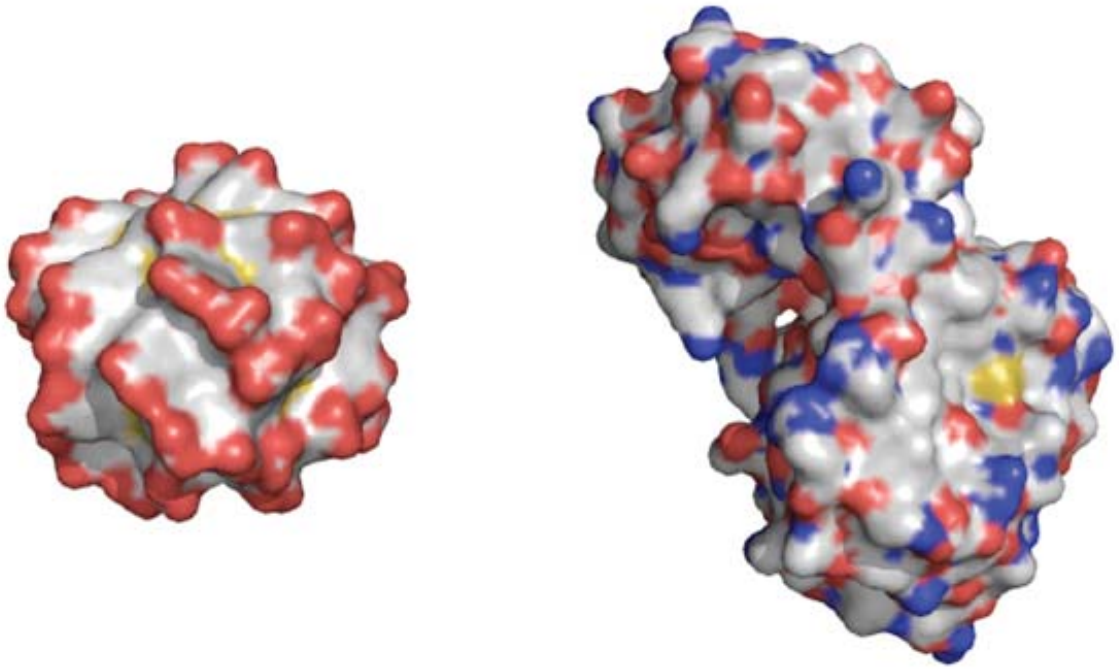

Figure 8. Surface Rendering of an X-ray Crystal Structure of a 15 kDa Protein and a 2.0 nm Gold Nanoparticle.

3.4. Interleukin-2/Interleukin-2 Receptor

Interleukin-2 (IL-2) is a 15 kDa cytokine that is a strong immunoregulatory lymphokine produced by T-cells in response to antigenic or mitogenic stimulation. IL-2/IL-2R signaling is required for T-cell proliferation and elicits the inflammatory response.[16] Inhibition of this protein/protein interaction therefore causes a reduction in the inflammatory

response, making it a sought after target for medical applications. Reducing tissue inflammation is highly beneficial for reducing pain, helping organ transplant patients, as well as asthma and arthritis patients live more enjoyable lives.

Previously the IL-2/IL-2R interaction has been mitigated with monoclonal antibodies.[3] Monoclonal antibodies are antibodies with a single molecular specificity, and have been successful in targeting protein/protein interactions. One successful monoclonal antibody that binds the IL-2R alpha receptor is Daclizumab.[17] This IL-2 receptor antagonist has been used effectively for a decade, but was recently pulled from the market due to manufacturing costs.[17] Despite the success of engineered proteins, smaller alternatives are more cost effective and favorable, specifically for their pharmacokinetic and delivery properties. Numerous attempts have been directed toward the development of small molecule antagonists of the IL-2/IL-2R interaction. Many potential drugs have been synthesized to inhibit this interaction.[18-21] Three known small molecule antagonists for IL-2/IL-2R interaction are depicted in **Figure 9**[3] however, none of these synthetic drugs have been approved for clinical use.

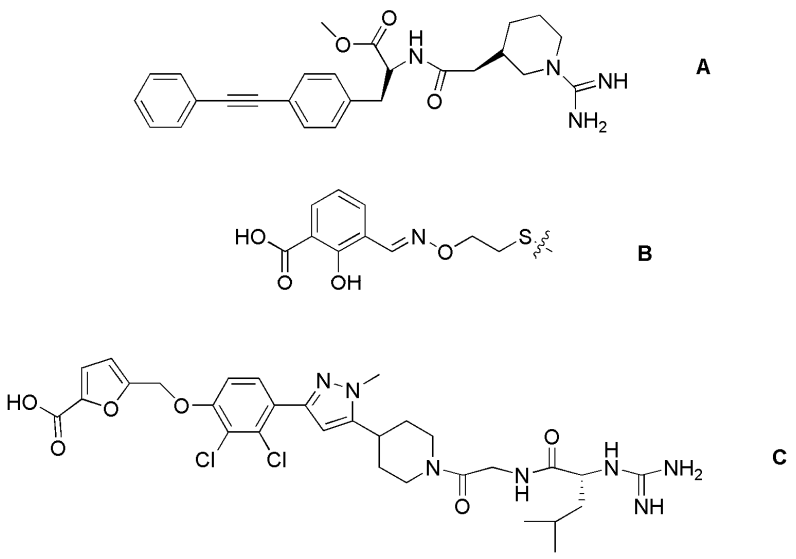

Figure 9. Synthetic Antagonists for IL-2/IL-2R.[3]

Compound **A** was chosen as the proof-of-principle ligand to attach to the gold nanoparticle because of the availability of a detailed NMR study of how **A** recognizes IL-2.[22] Compound **A** exhibits a K_d of 10 μM[18] to IL-2. Compound **A** however, is incapable of inhibiting the IL-2/IL-2R interaction, making it an ideal candidate for testing this proof of principle methodology of transforming weakly binding drugs into strongly binding drugs through conjugation to gold nanoparticles. The X-ray crystal structure of IL-2 in complex with **A** has been solved[19] (**Figure 10**), allowing us to utilize rational design to incorporate a linker and sulfur moiety on **A** for attachment to gold nanoparticles without altering the binding properties of the drug to IL-2. Compound **A** will now be referred to as compound **1** (**Figure 11**). Compound **1** has been shown to bind IL-2, instead of IL-2Rα.[18] This molecule

has an IC_{50} value of 3 μM against the IL-2/IL-2R interaction, indicating the ester modification does not negatively impact binding.[18, 22] The stereoisomer (compound **2**), is inactive against IL-2/IL-2R, making it an ideal compound for control experiments.

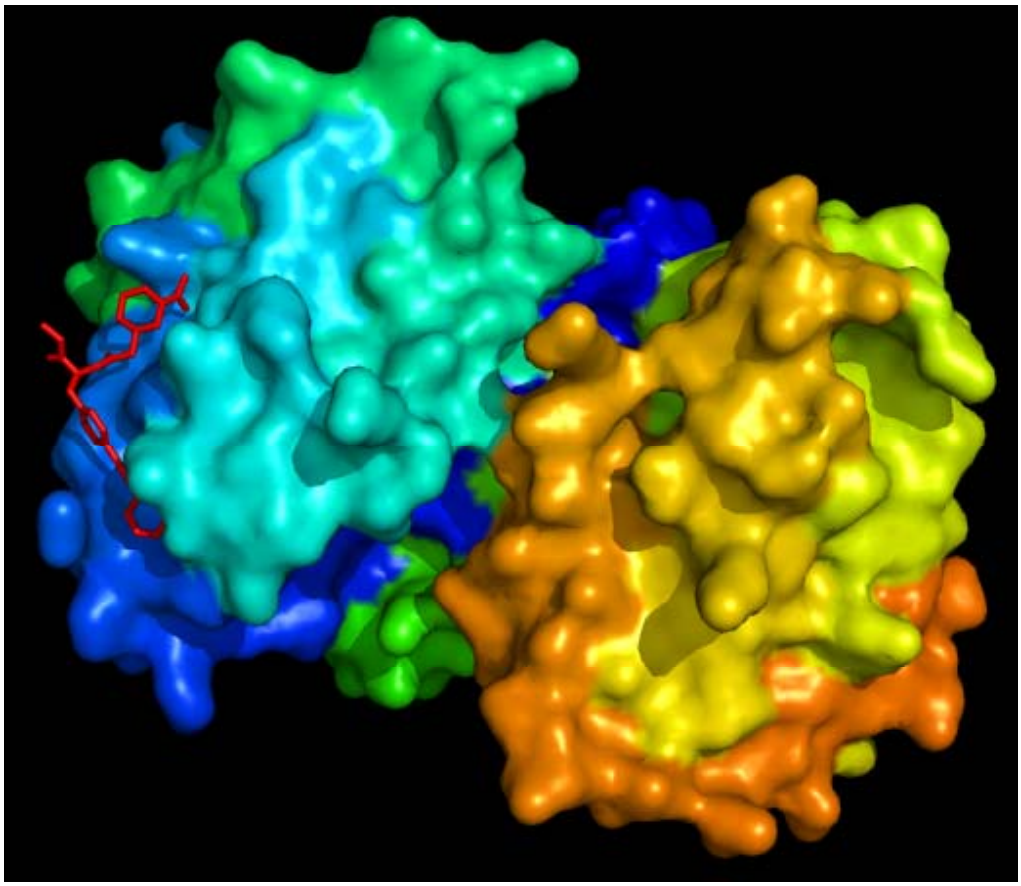

Figure 10. Surface Rendering of an X-ray Crystal Structure of Interleukin-2 with **1** bound. **1** is indicated in red.

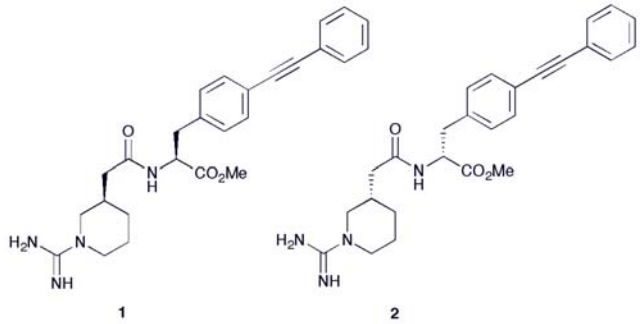

Figure 11. Base Compounds for IL-2/IL-2R Interaction.

The inability to efficiently disrupt the IL-2/IL-2R interaction may be rationalized by considering the relative size scale of **1** and the interface between IL-2 and IL-2R (**Figure 10**); **1** is simply too small and does not possess the requisite affinity to effectively disrupt the large contact area that occurs between IL-2 and IL-2R. Moreover, this problem is not unique to these proteins, and represents a general challenge for the design of therapeutics that target protein/protein interactions.

3.5. Our Method

In order to achieve size-comparability to the protein itself, we hypothesized that conjugating a derivative of compound **1** to a nanoparticle in a multivalent format will achieve the size we desire. In order to accomplish this, Dr. Wei Zeng synthesized two compounds, **3** and **4**, derivatives of compounds **1** and **2** with an oligoethylene glycol linker and a disulfide moiety (**Figure 12**) to facilitate attachment to gold nanoparticles.

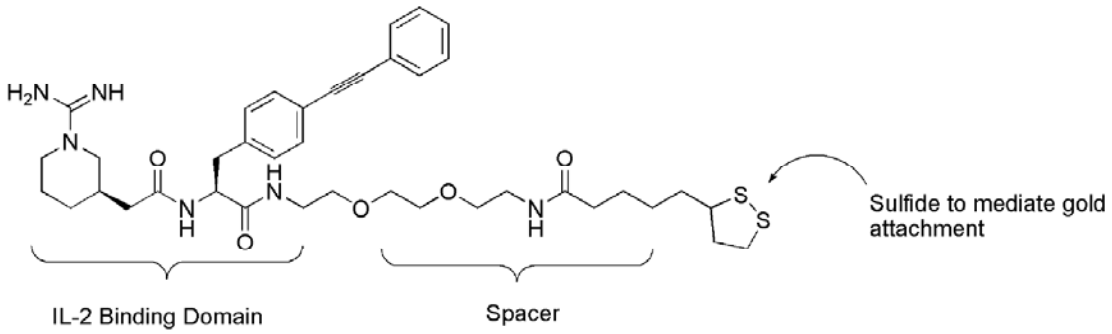

3

Figure 12. Active IL-2 drug with Linker and Disulfide for Nanoparticle Attachment; **4** is the enantiomer of **3**.

The specific goal of this research was to show that the attachment of weak binding drugs to the surface of a gold nanoparticle could increase the protein binding affinity in comparison to the drug alone. We have achieved this by synthesizing mono-dispersed gold nanoparticles and then coating them with drug analog **3**, which is known to inhibit the well-characterized IL-2/IL-2R interaction, and utilized the enantiomer of **3** as our control compound naming it compound **4**.

3.5.1. Synthesis of Gold Nanoparticles

The first step was to synthesize gold nanoparticles for attachment of compounds **3** and **4**. The gold nanoparticles (AuNP) protected by 4-mercaptobenzoic acid were synthesized using a modified single phase Brust synthesis.[23, 24] This modified synthesis was developed by Dr. Christopher Ackerson (Colorado State University) and gives molecularly dispersed particles without the need for purification.[25] This synthesis is unique because it

produces 1.5, 2.0, and 3.0 nm particles with a para-mercaptobenzoic acid monolayer in excellent monodispersity. We employed this procedure to synthesize 2.0 nm particles that have a proposed molecular formula of $Au_{144}(HSC_6H_4COOH)_{60}$. These particles have been characterized by transmission electron microscopy (TEM), a representative image is shown in **Figure 13**.

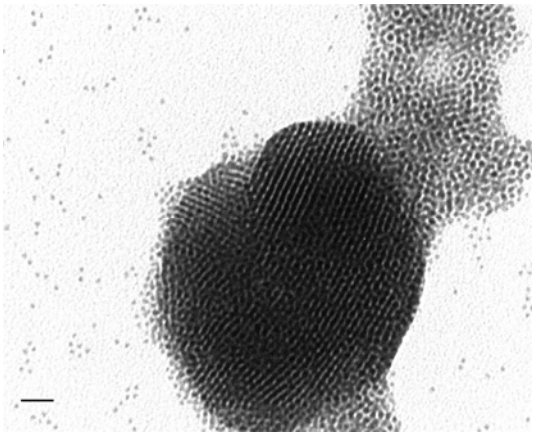

Figure 13. Transmission Electron Microscope Image of 2.0 nm para-Mercaptobenzoic Acid Protected Gold Nanoparticles with 10 nm Scale bar.

3.5.2. Synthesis and Characterization of Drug/AuNP Conjugates

Initially, place-exchange reactions of drug **4,** or the inactive enantiomer, onto the particles was performed by first reducing the disulfide bond of the drug with tris-carboxyethyl phosphine (TCEP) (**Figure 14**). This reaction can reduce disulfides efficiently but does not compete with free thiols (like dithiothreitol, a commonly employed disulfide reductant) in place-exchange reactions on gold.[26] The optimal concentration of TCEP was

determined to be 160 μM in a 0.5:1 feed ratio of TCEP:drug **4**. This was determined by running ten reactions simultaneously with a range of TCEP concentrations. Reactions that were too concentrated caused the dark purple (AuNP) solution to become colorless. This change was due to etching of the particle surface caused by a high concentration of thiol present in the solution. We used the highest concentration of TCEP that produced no color change. The reduced drug was added to 2.0 nm 4-mercaptobenzoic acid protected particles. The drug **4**:4-mercaptobenzoic acid feed ratios ranged from 0.25:1 to 32:1. A polyacrylamide gel electrophoretic analysis of these reactions is depicted in **Figure 15.** Feed ratios higher than 8:1 resulted in water insoluble product.

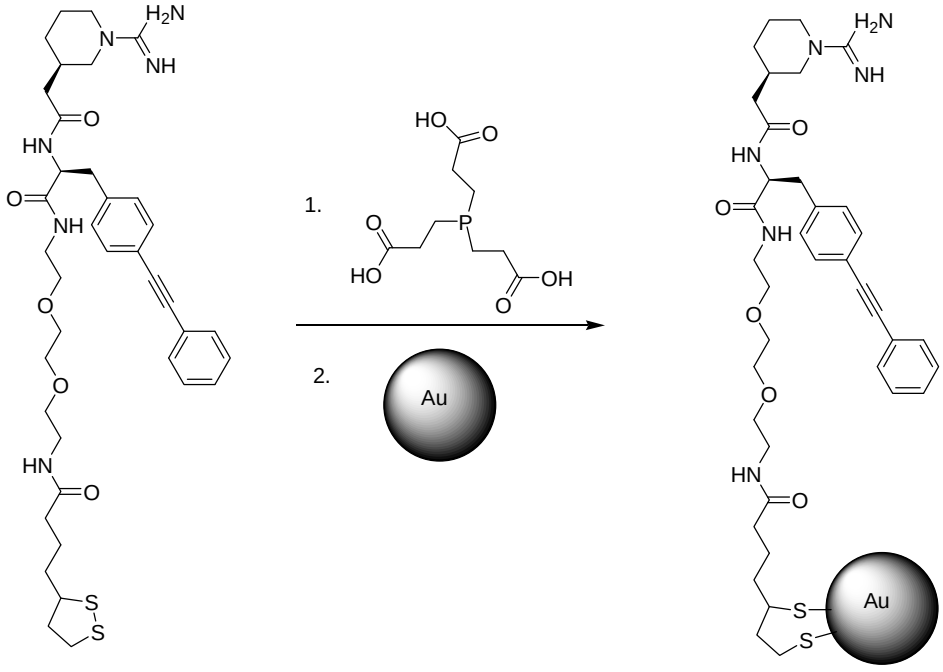

Figure 14. Reduction of Disulfide Bond on the Active Drug and Exchange onto p-MBA protected Gold Nanoparticles.

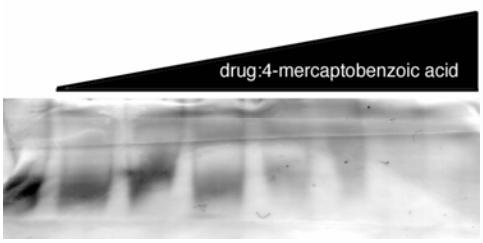

Figure 15. Effects of Drug **4**:(pMBA) Feed Ratio on 2.0 nm Particle Gel Mobility. Left to right, the Molar Feed Ratio of Drug **4**:pMBA was 0:1, 0.25:1, 0.5:1, 1:1, 2:1, 4:1, 8:1, and 16:1. Feed Ratios Higher Than 8:1 were Not Visualized Due to Aqueous Insolubility.

While investigating the physical properties of drug coated nanoparticles, we encountered numerous problems with aqueous solubility. In order to enhance the solubility of the drug-nanoparticle conjugate, we explored various solvent systems including water, TK buffer, TK buffer and glycerol, 10% SDS, 10% tween 20 and triton-x-100. However, none could successfully solublize the drug-coated nanoparticles. An alternative effort at increasing the aqueous solubility of these nanoparticle conjugates included employing a mixed monolayer of para-mercaptobenzoic acid (p-MBA) and other aqueous soluble thiols such as mercaptopropane sulfonic acid, 6-mercaptohexanoic acid, mercaptosuccinic acid, mercaptoundecane sulfonic acid and glutathione. Stellacci's group uses mercapto sulfonic acids, neither proved to increase aqueous solubility for our system.

Gratifyingly, we discovered that exchanging glutathione onto the p-MBA protected gold nanoparticles prior to the drug exchange reaction effectively solubilized the drug-coated nanoparticles in aqueous medium. In order to determine the optimal concentration of glutathione necessary for enhancing aqueous solubility after the drug exchange reaction was completed, we employed a 96 well plate screen varying the glutathione concentration on one axis and the reduced drug concentration on the other. The optimal feed ratio of

glutathione:p-MBA was determined to be 3.84:1. Once this was determined, the glutathione passivated particles were then used in place exchange reactions with the reduced IL2 active and inactive drugs **3** and **4**.

3.5.3. Quantitation of Drugs Conjugated to the AuNP

Upon successful place exchange reactions with **3** and **4** onto the glutathione passivated p-MBA protected gold nanoparticles, it was necessary to determine the number of drugs that were exchanged onto the nanoparticle. There are three basic ways to quantify drugs per nanoparticle: methanol precipitation of product, ultra violet - visible (UV-visible) spectroscopic estimation, and decomposition of the drug/nanoparticle conjugate.

3.5.3.1. Methanol Precipitation Protocol to Determine Drugs/AuNP

Initially, we explored the methanol (MeOH) precipitation method to quantify drugs/particle. After the drug exchange was complete, MeOH and NaCl were added to all reaction samples in order to dehydrate the particles and force precipitation. These samples are then spun in a centrifuge and the supernatants, which contain the free drugs that have not exchanged onto the nanoparticle, were removed and saved. This procedure was repeated twice more, the supernatants of each three precipitation steps were then combined and then UV-visible spectra were acquired on the supernatants. Using the molar extinction coefficients determined for the drug molecule and p-MBA, as well as the known initial

concentration of gold nanoparticles we calculated the number of drugs/particle, as seen in **Table 6**. The two major assumptions with this analysis were that the moles of gold nanoparticles at the beginning of the exchange and at the end of the work up are the same. The second assumption is that the total absorbance at 280 nm is due to p-MBA leaving the particle for IL-2 drug to conjugate, hence excluding the absorbance from unexchanged IL-2 drug, in turn over estimating the concentration of bound drug to the NP. In addition to this, the data we have to date on the synthesized p-MBA protected AuNP scaffold (2.0 nm) suggests there are only sixty ligand sites on the particle itself, therefore the calculated drugs/particle value of 76 for analyte 8 appears to be an over estimate. However this method is based upon assumptions and therefore these estimated averages need verification with an additional method.

Table 6. Drugs per Particle via MeOH Precipitations.

Sample Name	Feed Ratios (drug 3:PMBA)	Over Estimated Number of Drugs/Particle
Analyte 1	0:1	0
Analyte 2	0.03:1	1.16
Analyte 3	0.05:1	2.41
Analyte 4	0.11:1	4.7
Analyte 5	0.22:1	9.33
Analyte 6	0.43:1	18.6
Analyte 7	0.86:1	36.9
Analyte 8	1.72:1	76.2

3.5.3.2. Particle Decomposition Protocol to Determine Drugs/AuNP

Particle decomposition and the subsequent release of the particle-bound drugs was also employed to quantitate the average number of drugs per particle. This was attempted by adding KCN, β-mercaptoethanol (BME), thiomalate, tiopronin, and mercaptohexanoic acid to the drug coated NP solution. β-mercaptoethanol displaces the drug molecules from the particle surface and renders the resulting particle insoluble. β-mercaptoethanol, like all short-chain thiols, cannot effectively prevent irreversible flocculation of monolayer-protected gold nanoparticles. Following β-mercaptoethanol induced particle precipitation, UV-visible spectra were acquired on the supernatants after centrifugation. Using the molar extinction coeffiecients determined for drug **3** and p-MBA, in conjunction with the known initial concentration of gold nanoparticles, a 0.25:1 drug feed ratio particle was calculated to be an average of 13 drug molecules coordinated to the particle. This is an estimate because we cannot know that all drugs are released from the insoluble material that results from β-mercaptoethanol addition.

3.5.3.3. Overlapping Peak Absorbances - Protocol to Determine Drugs/AuNP

The final method we used to determine the number of drugs/AuNP was based on the overlapping UV-visible absorbances of the conjugated particle, the "naked" particle and the various ligands. The reaction mixture was methanol precipitated to removed any thiols not bound to the nanoparticle, the product was then resolubilized and measured

spectrophotometrically. The calculated Beer's law extinction coefficients for **3**, 2.0 nm gold particles, and *p*-mercaptobenzoic acid at 280 nm are 2.8×10^4 M^{-1} cm^{-1}, 8.6×10^5 M^{-1} cm^{-1}, and 3.26×10^3 M^{-1} cm^{-1}, respectively. Because only the gold core has appreciable absorbance at 510 nm, the absorbance at 510 nm was used to determine the concentration of the 2.0 nm gold particles. Since the extinction coefficients of **3** and the 2.0 nm gold particles are much larger than that of *p*-mercaptobenzoic acid at 280 nm, the problem was treated as a system of two absorbers rather than three.

Thus:

$$(1)\ A_{\text{total, 280 nm}} = A_{\text{[2.0 nm gold particles], 280 nm}} + A_{\text{3, 280 nm}}$$

$$(2)\ A_{\text{total, 280 nm}} = \varepsilon_{\text{2.0 nm gold particles, 280 nm}}\,[\text{2.0 nm gold particles}] + \varepsilon_{\text{3, 280 nm}}\,[3]$$

The assumption stated above is that term one on the right hand side of equation (2) does not change significantly when *p*-mercaptobenzoic acid ligands are replaced by **3** ligands on the surface of the gold nanoparticle. Thus, every term is known except [**3**]. Solving using measured absorbance values results in [**3**] = 333 μM, [2.0 nm gold particles] = 95 μM, therefore [**3**]/[2.0 nm gold particles] = 3.5 Drugs per nanoparticle. The same method was used to quantitate the number of **4** per nanoparticle.

3.5.4 Demonstration that the Drug Coated AuNPs bind to IL-2

We employed polyacrylamide gel electrophoresis (PAGE) to establish binding to IL-2 and ensure there was no aggregation of the particles after conjugation with the drug. **Figure 16** shows all drug/nanoparticle conjugates, regardless of drug load, penetrate the gel successfully and in tight band; therefore we can infer that there is no particle aggregation. The native PAGE gel in **Figure 17** gives visual evidence that the drug/nanoparticle conjugates bind to IL-2R. Lane 1 contains IL-2 only; lane 2 contains IL-2 and a 8:1 feed ratio drug coated nanoparticle; lane 3 contains IL-2 and a 0.5:1 feed ratio drug coated nanoparticle; lane 4 contains IL-2 and glutathione-coated nanoparticles; lane 5 contains the drug nanoparticle utilized in lane 2; lane 6 contains the drug nanoparticle utilized in lane 3; and lane 7 contains glutathione-coated nanoparticles. **Figure 17A** is the gel prior to staining. Drug coated nanoparticles are apparent in lanes 2-7 as expected. Gold nanoparticles bound to IL-2 are faintly apparent at the top of lane 2. **Figure 17B** is an image of the top of the gel cut off and stained with Coomassie (protein stain). Protein bands are visible in lanes 1-4. A gel shift to faster mobility is noted for IL-2 in lane 2, due to a decreased mass/charge ratio upon drug nanoparticle binding. **Figure 17C** is an image of the same part of the gel shown in panel (B), however the Coomassie stain was removed and the gel was restained with an autometallographic stain that reveals only gold nanoparticles. The presence of drug/nanoparticles bound to IL-2 in lanes 2 and 3 are confirmed. Control particles prepared without drug do not bind to IL-2, as seen in lane 4.

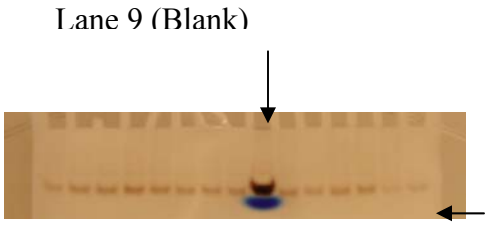

Figure 16. Drug/Nanoparticle Conjugates Traveling into an Acrylamide Gel and the Blank (p-MBA coated NP) in lane 9.

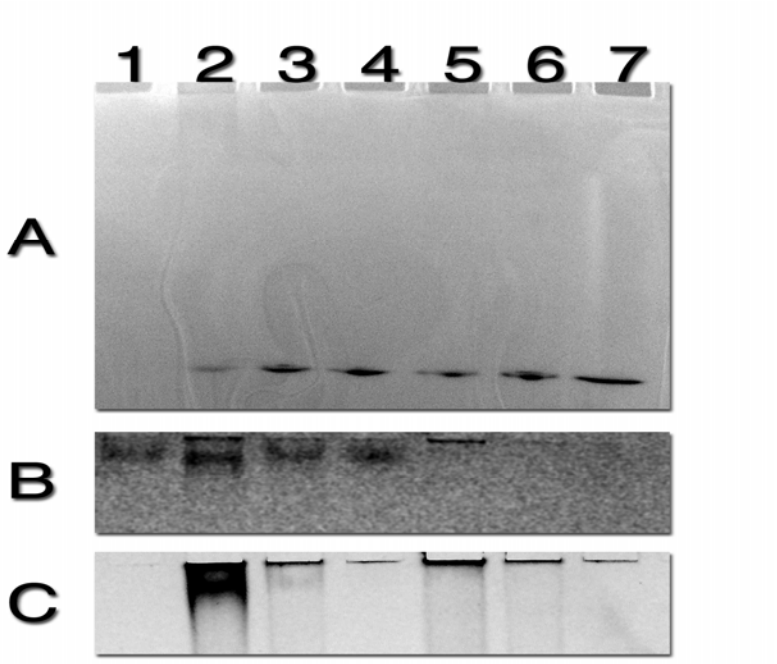

Figure 17. Drug/nanoparticle (DNP) IL-2 binding visualized non-denaturing PAGE. Lane: 1. IL-2; 2. IL-2 + 8:1 feed ratio DNP; 3. IL-2 + 0.5:1 feed ratio DNP; 4. IL-2 + Glutathione-coated NP; 5. DNP from lane 2 only; 6. DNP from lane 3 only; 7. Glutathione-coated NP. (**A**) Gel prior to staining. (**B**) Coomassie stain of (A). (**C**)An autometallographic stain of (A).

3.5.5. Biophysical Characterization - Biacore

The use of optical Biosensors has been growing since their advent. Dr. David Myszka at the University of Utah; is a pioneer as well as a leader in the field of optical biosensors. Every year a review of the commercial optical biosensor literature is published by the Myszka group (**Figure 18**). To date there about over 30 manufacturers of biosensor instruments employing Surface Plasmon Resonance (SPR), or alternative optical detection methods.[27]

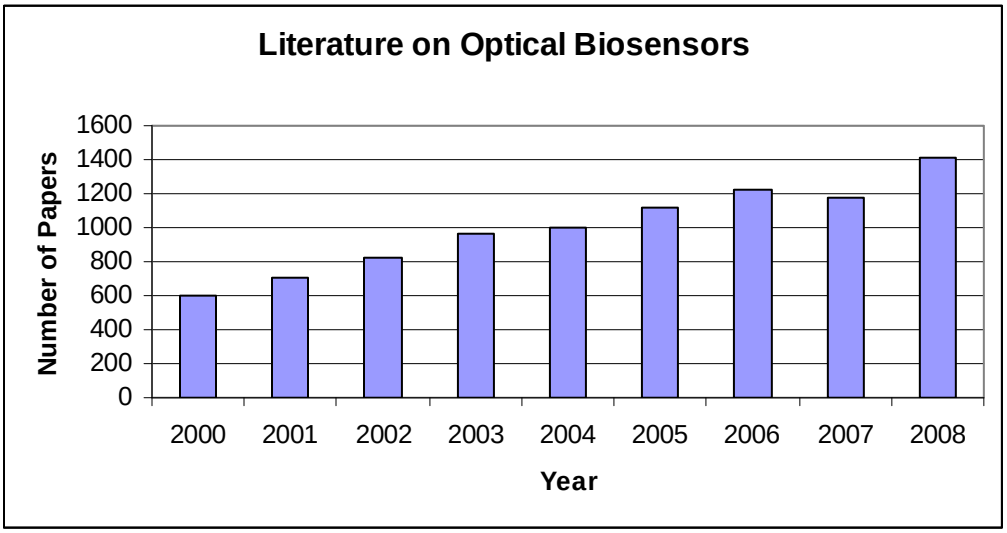

Figure 18. Number of Published Papers Utilizing Commercial Optical Biosensors in the last 9 years.

To explore the kinetic rate of this interaction we utilized Biomolecular Interaction Analysis using Surface Plasmon Resonance (Biacore).

The Biacore analysis for affinity was employed on a Biacore 2000 and also a Biacore T100. Standard amine coupling conditions; NHS (N-hydroxysuccinimide) and EDC (N-ethyl-N'(dimethylaminopropyl)carbodiimide) were employed to activate the dextran surface to bind IL-2 onto the sensor chip.

3.5.5.1. Biacore 2000 Analysis – Surface Plasmon Resonance Analysis

Due to the complicated kinetic analysis of polyvalent interactions studied by SPR, this analysis was restricted to equilibrium binding analysis. This data is comprised of 8 different preparations of drug/AuNP conjugate. One of the preparations, referred to as analyte 1, has no drug. Analyte 2 is estimated to have 1 drug per particle. Analytes 3 – 8 have increasing amounts of drug/particle. As discussed in section **3.5.3.1** and **3.5.3.2,** there is a clear systematic error in the determination of drugs/particle (**Table 6**). During this BIAcore analysis, we observed no problems with insolubility for the highest drug load particles used. Given that we have observed insoluble products at high drug feeds, this indicates that we did not characterize the highest drug loads possible because we never reached an insoluble product.

We attempted to record steady state equilibrium data on eight preparations of drug/nanoparticle, with drug loads ranging from 0 to 76 drugs/particle determined via the MeOH precipitation method (**Table 6**). Each of the eight preparations was injected over a Biacore CM5 sensor chip with 4 flow cells. Each flow cell (FC) was loaded with a different

amount of IL-2; FC1 had 800 response units (RU) of IL-2 immobilized on the surface, FC2 had 400 RU, FC3 had 200 RU, and FC4 was a no-IL-2 control surface.

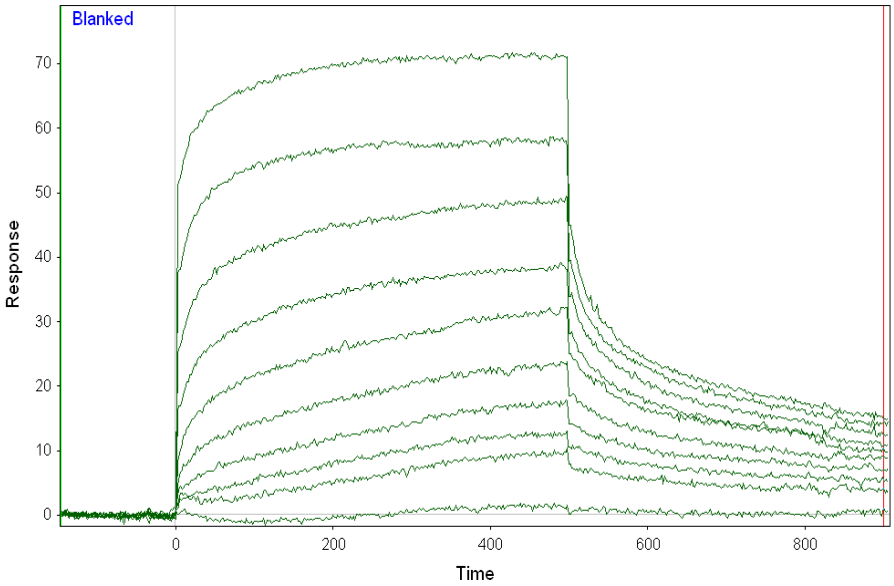

Figure 19. Analyte 8 over Flow Cell 1.

Figure 19 shows the response on FC1 to the highest drug load particle, analyte 8, at 10 different concentrations depicted with green sensograms. The response on FC4 (no IL-2) was subtracted from this data. For most concentrations of analyte 8, the data appears to be reaching steady state kinetics, indicated by the linear appearance of the sensogram by the end of the injection; thus indicating the applicability of analyte 8 to fit a steady state model. The plot shown here has the highest responses of all the particles tested in this run (these "highest drug load" particles appear to have the highest affinity), but all the other analytes (with lower drug feeds) behave in a similar manner. A plot of all analytes over all surfaces is shown in

Figure 20. One concern about this data set is that the binding of the "no drug control" particles is almost twenty-five RU for the highest concentration (**Figure 21**).

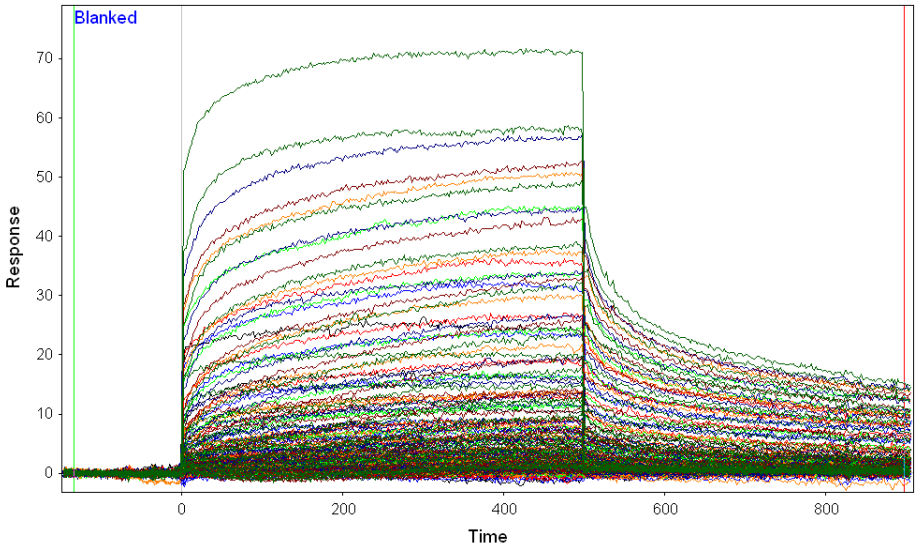

Figure 20. Sensograms of All Analytes Injected Over All Four Flow Cells.

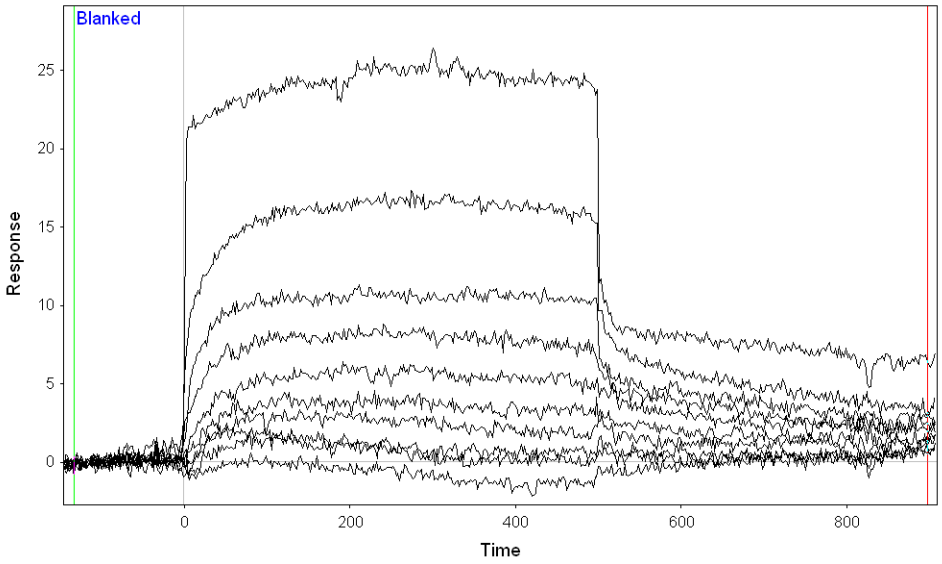

Figure 21. Glutathione Coated Nanoparticles on Flow Cell 1.

Fitting isotherms to the binding data with the commonly used program Scrubber©, developed by Dr. David Myszka, enables the calculation of affinity constants. Scrubber© can account for up to two independent binding sites in the isotherm fit. The 1:1 langmuir model fits the steady state data for "low-drug-load" particles (Analytes 1, 2 and 3) but an increasingly poor fit as the drug load increases (Analytes 4-8), this is evident in **Figure 22**.

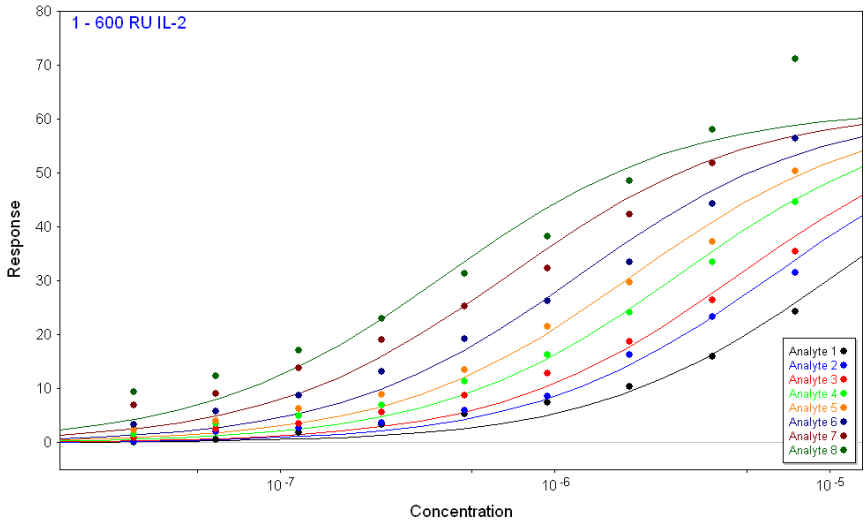

Figure 22. 1:1 Binding Model of all 8 Analytes.

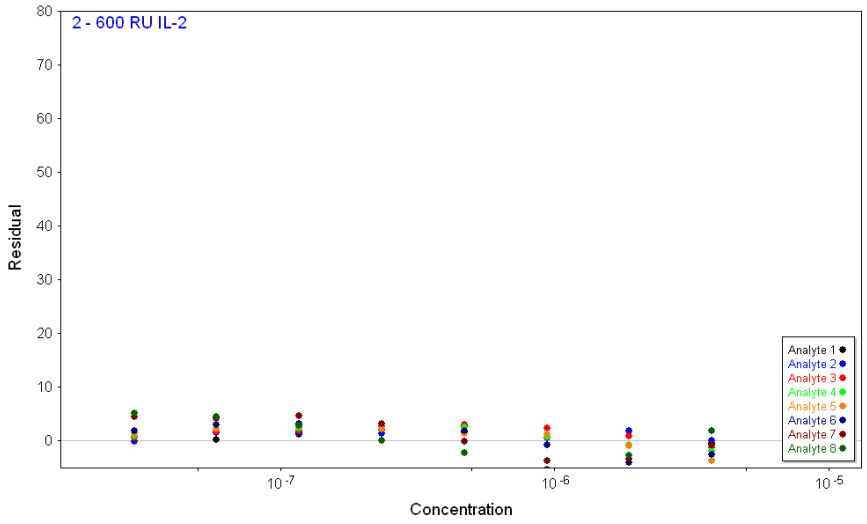

Figure 23. Residuals of the 1:1 Binding Shown in **Figure 22**.

Scrubber analysis attempts to subtract buffer readings (as blanks) from all sensograms to "clean" up the data and remove spikes. In our data collection we used glutathione coated particles (no drug control particles) as the subtractable buffer blank. Once the blank is subtracted from the sensograms we are theoretically left with fit-able curves. Therefore, one logical conclusion is that we are observing multiple binding events for nanoparticles with a large number of drugs.

The K_d values generated from each of these fits are shown in **Table 7**. Analyte 1 is the gold nanoparticle that has no drug on it, analyte 2 is estimated to have one drug per particle. The K_d generated with Biacore data for analyte 2 has a very close affinity to the drug by itself. Over the entire range of analytes, from one drug to a high drug load, the K_d spans a range a little bit larger than an order of magnitude.

Table 7. Dissociation constants based on Biacore data and Scrubber fitted.

Sample Name	Over Estimated Number of Drugs/Particle	K_d
Analyte 1	0	10.4 μM
Analyte 2	1.16	6.2 μM
Analyte 3	2.41	4.64 μM
Analyte 4	4.7	2.80 μM
Analyte 5	9.33	1.93 μM
Analyte 6	18.6	1.22 μM
Analyte 7	36.9	680 nM
Analyte 8	76.2	398 nM

Next we modified the fit so that two binding sites are considered for analytes 4-8, this is shown in **Figure 24**. As illustrated below, the 2:1 binding model fits the higher drug load analytes (analytes 4-8) better than the low drug load analytes (analytes 1-3).

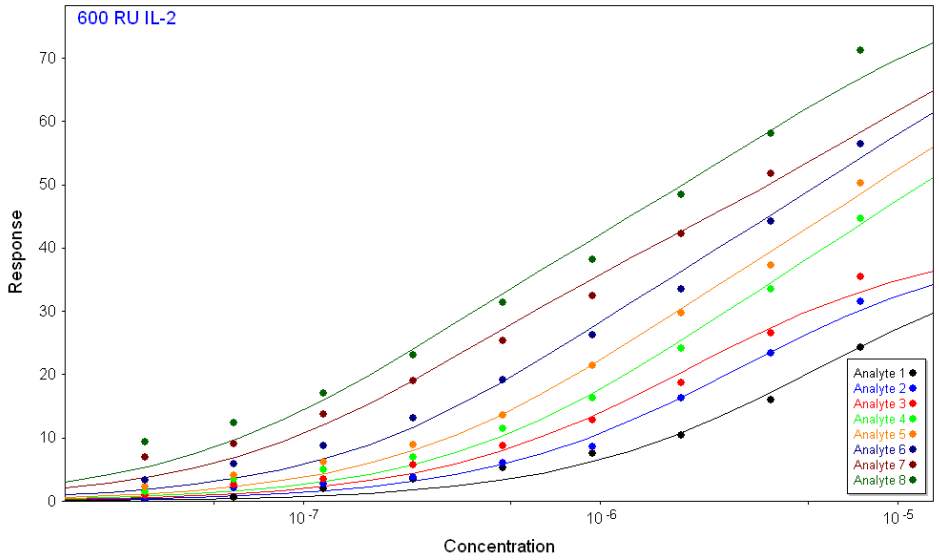

Figure 24. 2:1 Binding Model of All Analytes.

The fit from **Figure 24** produces the following K_d values in **Table 8**. The two K_d values reported for analytes 4, 5, 6, 7 and 8 represent a calculated K_d value for each binding site. In the case of analyte 8, the fit is beginning to diverge, probably because there is at least one third independent binding within this data. Again, the calculated K_d values span just over an order of magnitude – from 2.9 μM for an analyte with 1 drug/particle to 211 nM for the higher affinity site of a multivalent particle.

Table 8. 2:1 Dissociation Constant Values for Analytes 4-8, and 1:1 Dissociation Constants for Analytes 1-3.

Sample Name	Data Fit to a 1:1 Model or 2:1 Model	K_d
Analyte 1	1:1	5.4 μM
Analyte 2	1:1	2.9 μM
Analyte 3	1:1	1.98 μM
Analyte 4	2:1	1.59 μM 27.2 μM
Analyte 5	2:1	1.07 μM 19.1 μM
Analyte 6	2:1	660 nM 12.5 μM
Analyte 7	2:1	308 nM 9.86 μM
Analyte 8	2:1	211 nM 4.52 μM

This data was analyzed with three different approaches to evaluating equilibrium data. One approach – using 1:1 langmuir binding isotherms (**Figure 22**) – produces reasonable fits to the data for low drug loads (1 drug/AuNP) but produces poor fits for high drug loads. In all cases, the affinity appears to increase with increasing drug load. Another approach, which incorporates a 2:1 isotherm for the higher drug loads and a 1:1 isotherm for the lower drug loads, produces substantially better fits (**Figure 24**). The third analysis was preliminary, and has incorporated two changes which may improve upon the original analysis. One change is the subtraction of no-drug-control data from each of the drug-containing runs. The other change is that data from flow cells containing less IL-2 is

considered, this should decrease the polyvalent contribution to the data, as the ligand density may not be high enough for most analytes to bind more than one molecule of IL2.

Two major concerns arise in the above analysis: 1) the binding of the no-drug control and 2) and the tenuous nature of the analysis of multiple independent binding sites, and will be further explored in the future. Both analyses of the equilibrium data are summarized below:

Table 9. Initial K_d summary.

Analyte	K_d with 1:1 isotherm	K_d by 2:1 isotherm for 4-8; Global fit causes adjustment of values for 1-3
1 (No drug)	10.4 μM	5.4 μM
2 (1 drug/particle)	6.21 μM	2.90 μM
3	4.64 μM	1.98 μM
4	2.80 μM	1.59 μM
5	1.93 μM	1.07 μM
6	1.22 μM	660 nM
7	680 nM	308 nM
8 (high drug feed)	398 nM	211 nM

3.5.5.2. Biacore T100 Analysis with Dialed in Drugs per AuNP

After the initial round of experiments, we determined that an accurate measurement of drugs/AuNP was a high priority and that through advances in instrument/analysis software

and experimental design, K_d values could be obtained through a vigorous Biacore analysis alone.

It was determined the reduction of the disulfide bond of compound **3** and **4** was not necessary prior to the exchange reaction. Therefore exchanges to glutathione passivated nanoparticles were pursued in different buffer systems (100 mM Tris-HCl pH ~10, PBS, Borate, and 75% MeOH/12.5%Glycerol) in an attempt to obtain the highest aqueous soluble drug coated nanoparticles possible. Once this was achieved we implemented the overlapping peak absorbance method discussed in **Section 3.5.3.3** for quantitation of drugs/AuNP (**Figure 25**).

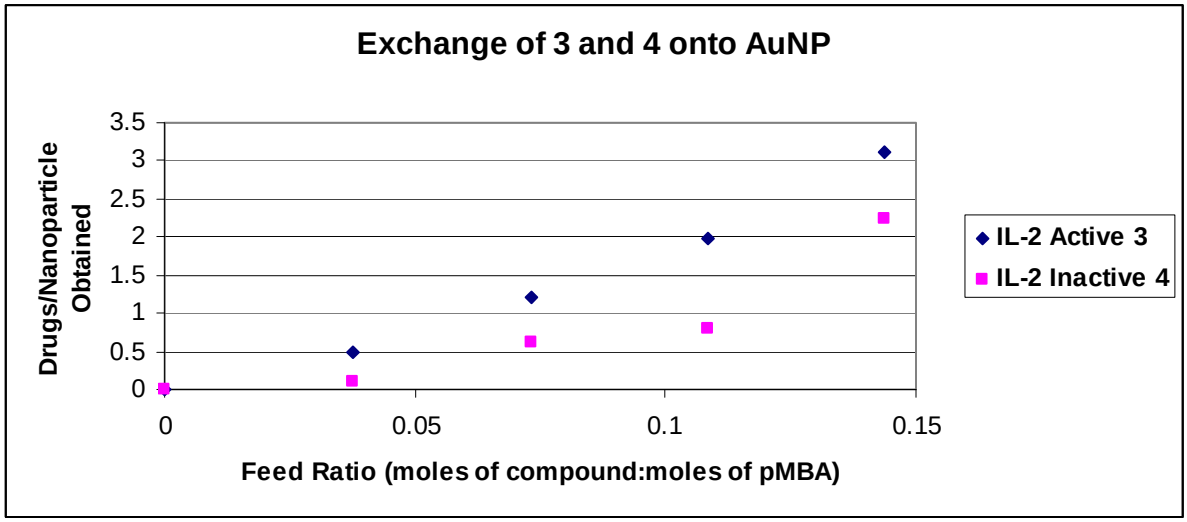

Figure 25. Drugs per Nanoparticle Obtained and Corresponding Feed Ratio.

These conjugates were then utilized for analysis on a Biacore T100. The experimental set up was similar to that used with the Biacore 2000. The standard amine coupling conditions were utilized to immobilize IL-2 on the surface of the flow cells.

The first set of experiments were performed with the three drug (**3**)/AuNP active conjugates and the affinity to IL-2 was determined and attempted to be simplified (from a multivalent system to a 1:1 system). The simplification was made possible by immobilizing low levels of IL-2. The following figures show data and analysis from Biacore T100 and Biacore T100 evaluation software. Flow cell one was a blank reference cell, flow cell two through flow cell four had increasing RU levels of IL-2 immobilized from 29 RU on flow cell two to 93 RU on flow cell four, all data was subtracted with flow cell one (the reference cell) and then analyzed.

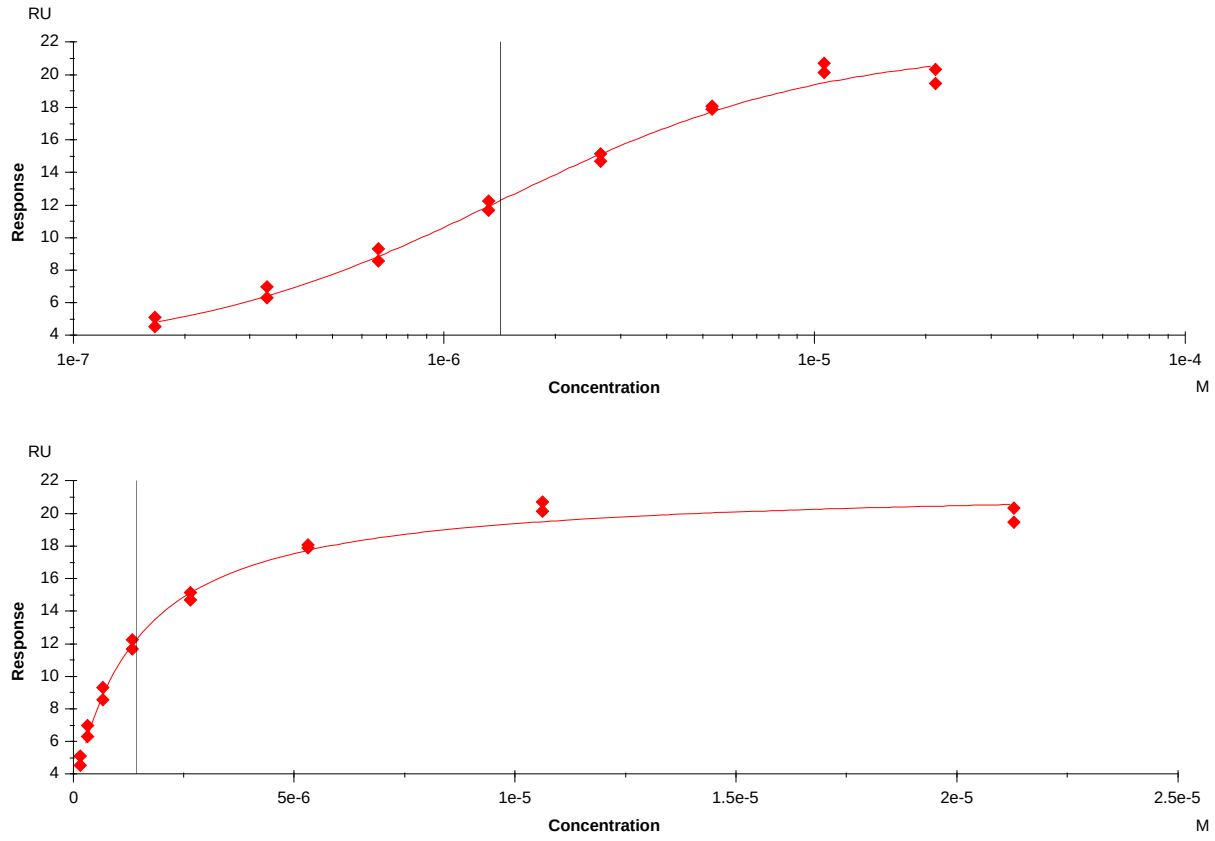

Figure 26. Binding Isotherms for Flow Cell 2.

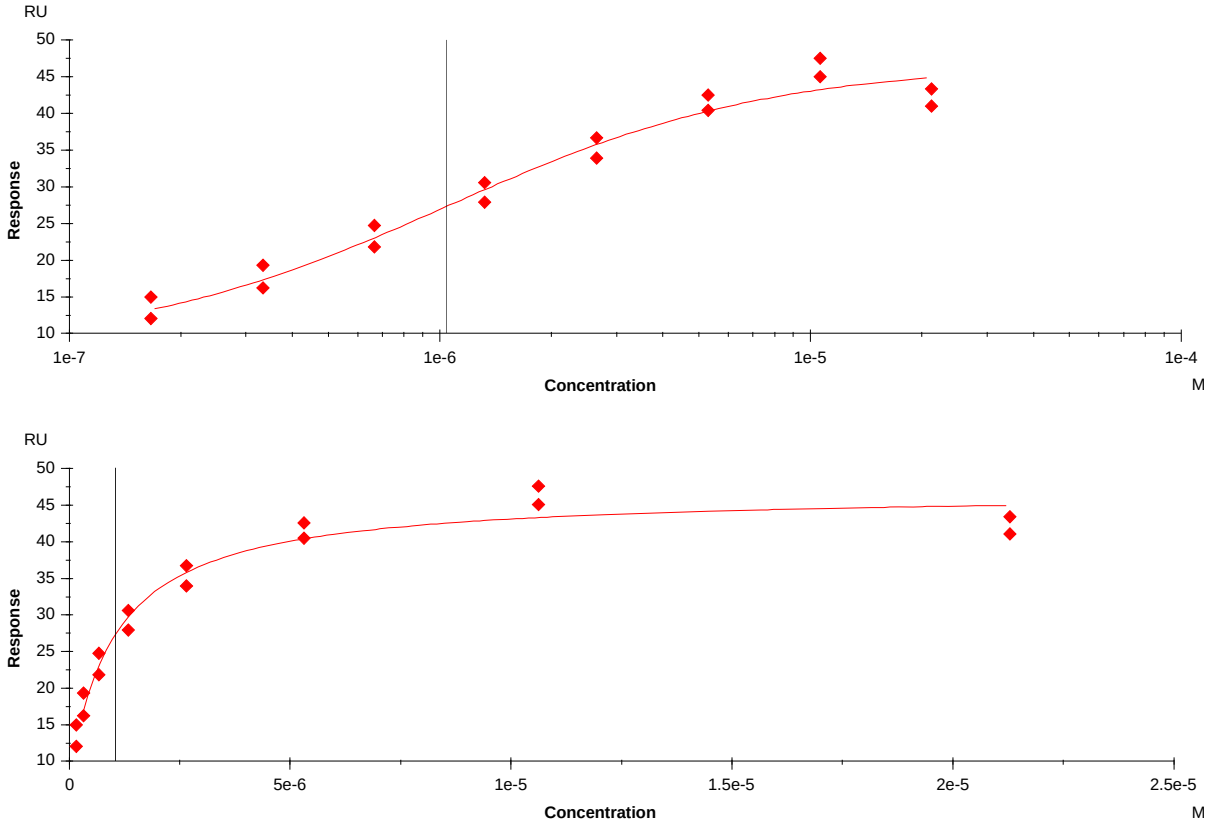

Figure 27. Binding Isotherms from Flow Cell 3.

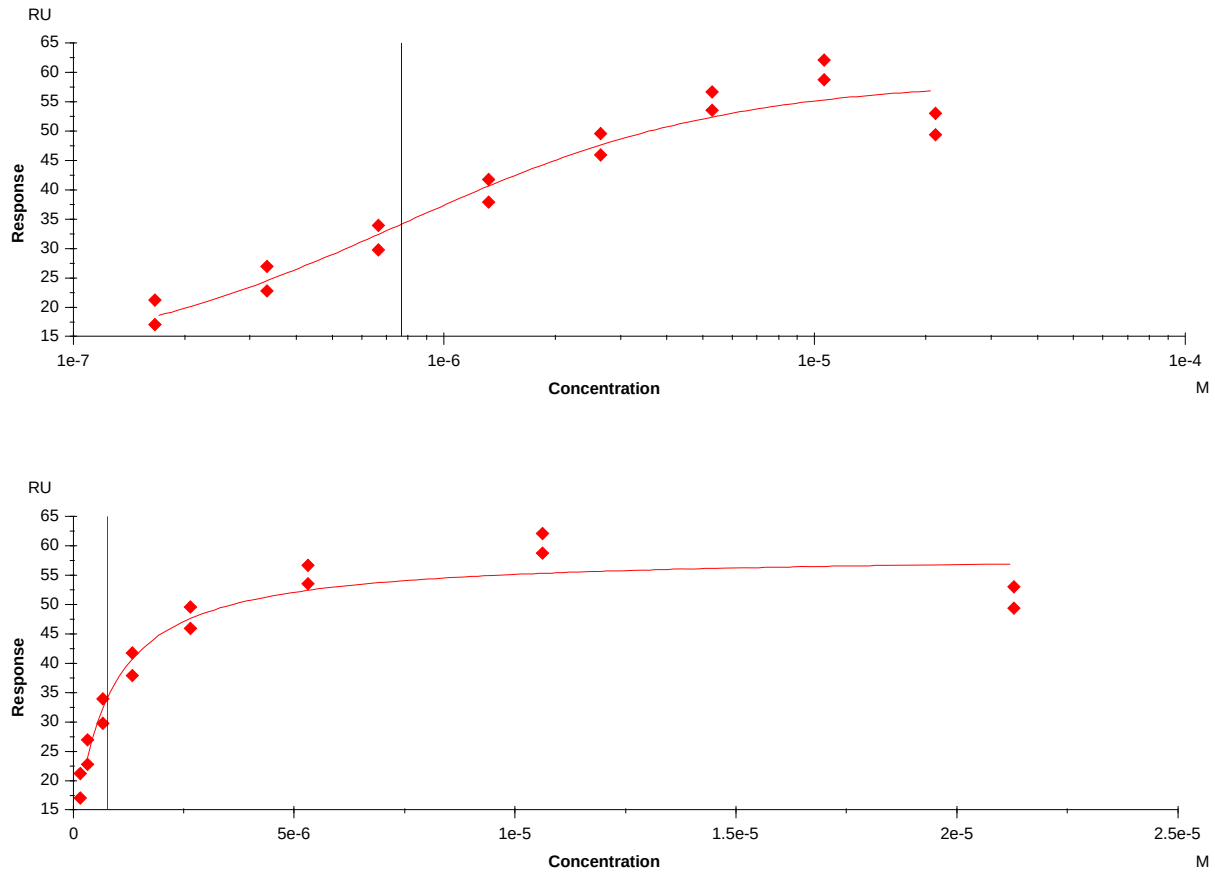

Figure 28. Binding Isotherms from Flow Cell 4.

The K_d values determined by Bia evaluation software indicates roughly the same binding affinity for all three flow cells. This signifies there is a low enough IL-2 coverage on all flow cells to be deemed a 1:1 binding regime. **Table 10** summarizes Bia evaluation values, showing K_d values for each flow cell, Chi^2, and maximum RUs for the drug conjugate over each flow cell.

Table 10. Summary of Bia Evaluation Data for **3**-NP over IL-2 Immobilized Flow Cells.

Flow Cell	K_d - μM	Chi^2	R_{max}
2	1.75	0.158	19.7 RU
3	1.50	0.44	40.9 RU
4	1.33	0.44	51.8 RU

Table 10 justifies the hypothesis that a low loading of IL-2 on the chip surface would simplify the binding kinetics. The binding isotherms depicted in **Figures 26**, **27** and **28** all show good fits to a 1:1 system. This indicates that the variable RUs of IL-2 on each flow cell was minimal enough to eliminate multivalent binding. However, proximity binding is still worth considering for the slight increase in affinity with the implementation of a gold nanoparticle scaffold. Next we tested the active IL-2/NP conjugates and the inactive IL-2/NP conjugates, **3**-NP and **4**-NP, respectively.

While implementing the low RU load of IL-2 on the surface of flow cell 2 and flow cell 4 and leaving flow cell 1 and 3 blank for reference, **3**-NP and **4**-NP were tested to rule out non-specific binding due the particle itself. The NP conjugates were prepared with a feed ratio that would obtain an average of 3 drugs/particle for both compound **3** and **4**.

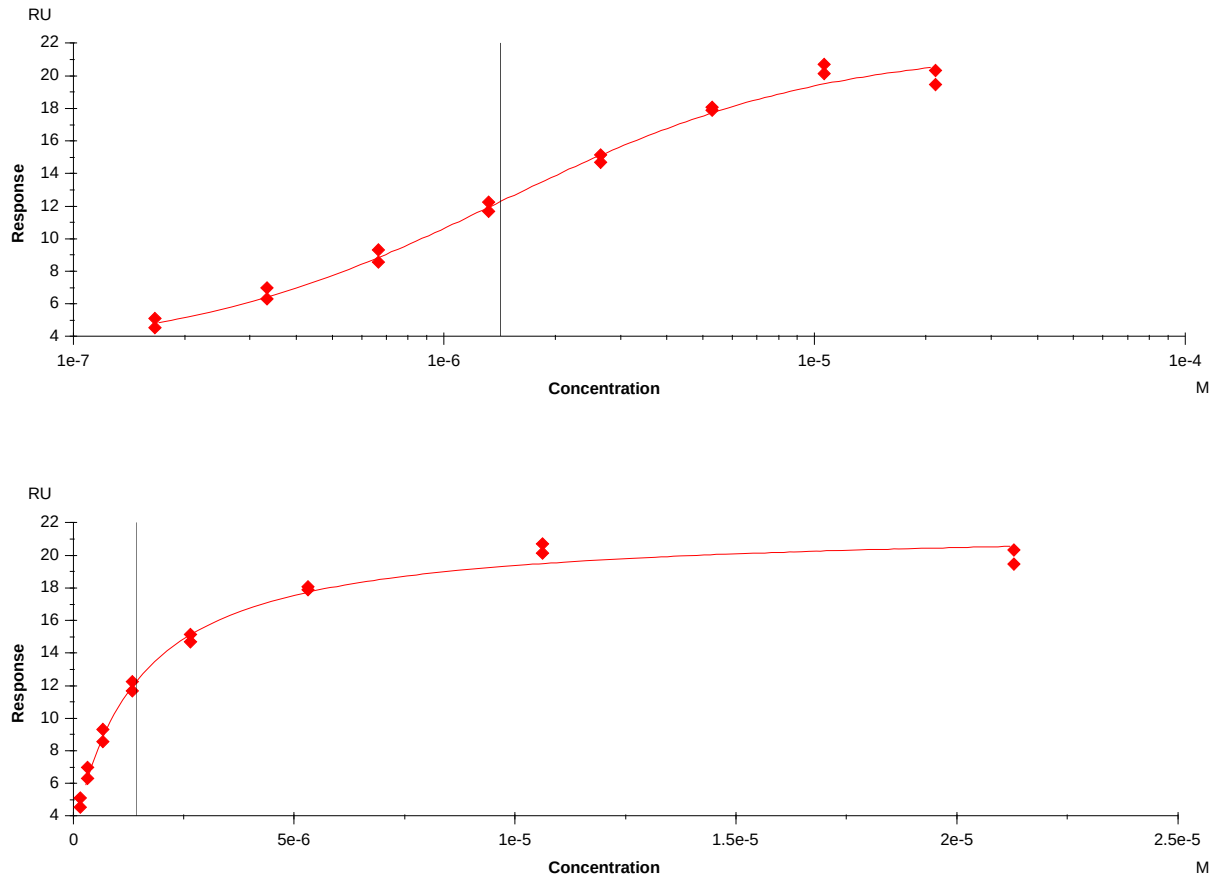

Figure 29. Binding Isotherms for Active Nanoparticle Conjugate, **3**-NP over a low RU of IL-2.

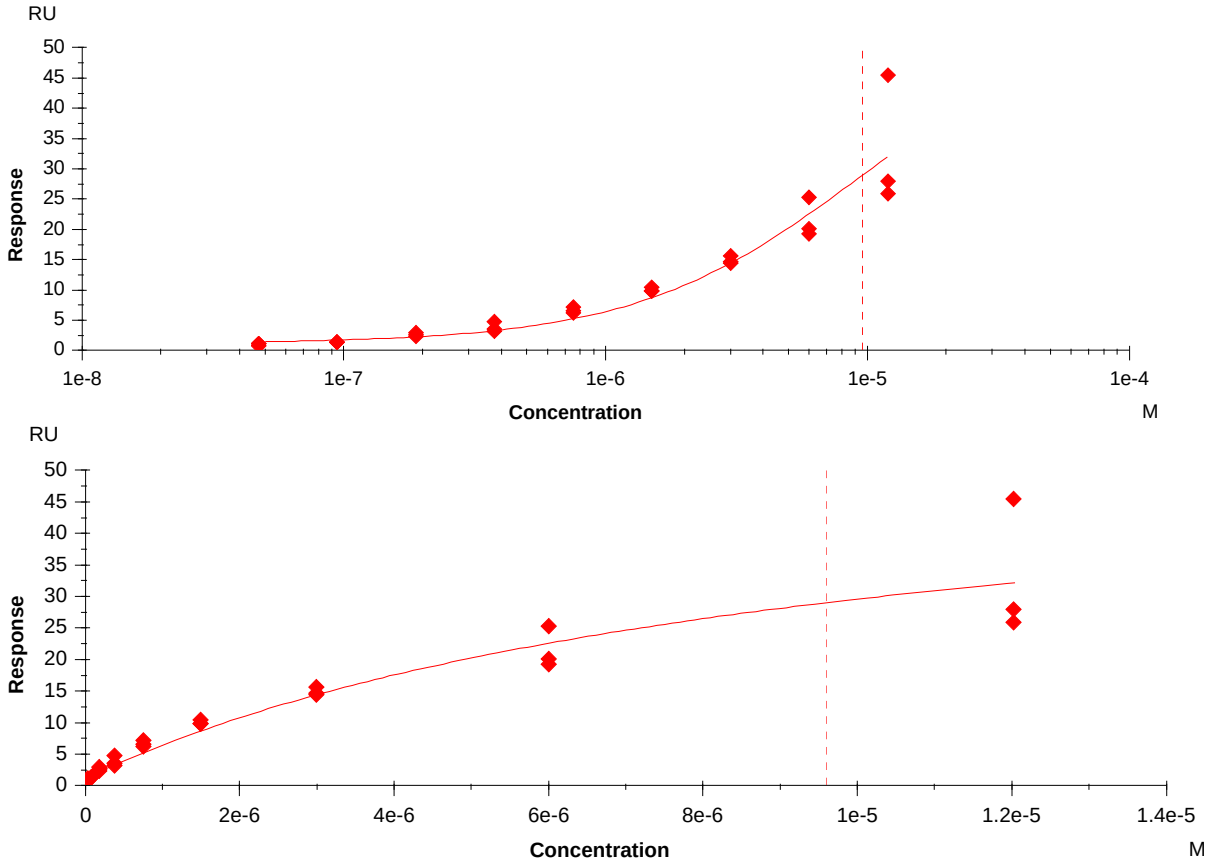

Figure 30. Binding Isotherms for the Inactive Conjugates, **4**-NP over a low RU of IL-2.

Table 11. Summary of final K_d values for **3**-NP and **4**-NP.

Sample	K_d - μM	R_{max}
3-NP	1.42	18.9 RU
4-NP	9.6 *not accurate due to failure to reach equilibrium	55.6 RU

It is clear from **Figure 30** that the **4**-NP (inactive np conjugate) does not bind with the same efficiency as **3**-NP (**Figure 29**). These isotherms indicate that the particle is not

involved in binding, and the conjugation of **3** and **4** to the gold nanoparticle still maintains the efficacy of the compounds themselves. The use of the nanoparticle scaffold slightly increased the binding affinity of the active (**3**) compound/nanoparticle, however the inactive (**4**) still remains an ineffective binder to IL-2, even when conjugated to a nanoparticle (**Table 11**).

3.6. Conclusion

In conclusion, we have shown that it is possible to use a structure-based approach to design small molecule coated gold nanoparticles that target IL-2. Furthermore, this general method to target protein/protein interactions using drug-coated nanoparticles could have potential towards many biological applications. There are upwards of 10,000,000 different proteins in the human body at a given time;[2] with >99% of them carrying out their biological function via protein/protein interactions. The ability to target a specific protein/protein interaction would allow virtually every protein in the human body to be utilized as a potential target for therapeutic intervention. Interfering with protein/protein interactions is a difficult challenge for drug discovery efforts, as protein surface areas are large, and multiple points of contact can be formed between two proteins. The size comparability that a drug-coated gold nanoparticle has in comparison to a protein potentially allows it to compete with protein/protein binding and it presents the ability for multiple binding ligands to at least one of the target proteins. This overall strategy combines the cell

permeability of synthetic organic drugs with the size and multivalency of gold nanoparticles and tests them as potential protein therapeutics.

In an effort to prove our hypothesis we have fabricated gold nanoparticles (average core diameter of 2.0 nm) conjugated to a drug analogue that binds IL-2. We have quantitated the average ligand coverage, and have confirmed that these drug-nanoparticle conjugates are soluble in aqueous solutions. We have also demonstrated that our conjugates bind to their IL-2 target by gel shift analysis, and two Biacore analyses. Our data suggests the multivalent nanoparticle has increased the K_d either through multivalent or proximity binding.

3.7. Experimental

Preparation of 2.0 nm gold particles

A concentrated gold-thiol polymer stock solution composed of 1 mM $HAuCl_4$, 3.4 mM 4-mercaptobenzoic acid, and 50% aqueous methanol was adjusted to pH ~13 using sodium hydroxide. This solution was allowed to stir overnight at ambient temperature in a sealed vessel. The solution was subsequently diluted to a final Au(III) concentration of 10 μM with the addition of methanol and water. Sodium borohydride (10 mM, aqueous) was added in a 3:1 molar ratio and after 16 hours of reaction time methanol was added to the reaction to precipitate the product. The product was collected by filtration, dissolved in water and then precipitated with methanol to obtain 2.0 nm gold particles.

Preparation of (GSH-NP)

2.0 nm gold particles (200 μM, 1.8 μmol) in H_2O and glutathione (GSH) (20 mM, 414 μmol) in 100 mM Tris were combined, and allowed to react at ambient temperature on a shaker rotisserie for 3 days. The product was precipitated and washed with methanol (3x) and collected by centrifugation at 6000 *g* to obtain GSH-NP. The GSH-NP was then re-suspended in 50% aqueous glycerol.

Preparation of ((3)-NP) and ((4)-NP)

GSH-NP (121 μM, 198 nmol) in 75% MeOH/12.5% H_2O/12.5% glycerol and compound (**3**) (24 mM, 1.48 μmol) in 75% MeOH/12.5% H_2O/12.5% glycerol was added. Different molar ratios of compound to p-MBA were used to obtain different drug per nanoparticle loadings, see **Table E1**. After 36 hrs, the supernatant was removed and the product was washed with methanol (3x) to remove excess compound (**3**) and displaced GSH to obtain (**3**)-NP. Pure (**4**)-NP was prepared as described above.

Table E1. Molar Feed Ratios Required to Obtain Specific Drugs/NP

[GSH-NP]	Moles NP	Molar Ratio Compound : pMBA	[Compound]	Moles Compound	Desired Drugs/NP
121 μM	198 nmols	0	24 μM	0	0
121 μM	198 nmols	0.037	24 μM	390 nmols	1
121 μM	198 nmols	0.073	24 μM	755 nmols	2
121 μM	198 nmols	0.108	24 μM	1.12 μmols	3
121 μM	198 nmols	0.144	24 μM	1.48 μmols	4

Transmission electron microscopy

5 μL of a solution of 2.0 nm gold particles was dispensed onto a 400 mesh carbon coated copper TEM grid (Electron Microscopy Sciences). The NP sample was allowed to incubate on the grid for 1 minute and then side-blotted with a Kimwipe. Then the grid was washed with 5 μL of milli-q treated H_2O, and side blotted with a Kimwipe. The grid was examined in a FEI CM12 microscope, operating at 100 kV accelerating voltage.

Biacore T100

All consumables were purchased from Biacore. Dock a S-series CM 5 chip, flow HBS-EP buffer, and prime the chip (4x). Normalize the chip surface with a nine minute injection of 70% glycerol, followed by another prime (4x). Set up a manual run to

precondition, over flow cells 1-4 with a 100 µL per minute flow rate, inject 50 mM NaOH for 12 seconds (2x), 0.1% HCl for 12 seconds (2x), 0.5% SDS for 12 seconds (2x), and 0,085% H_3PO_4 for 12 seconds (2x). Stop manual run, prime (5x).

For immobilization, start manual run over flow cells one and two with a 10 µL per minute flow rate. Premix 150 µL of NHS and EDC, inject this mix for seven minutes. Switch to flow cell two only, inject IL-2 (50 µL of a 1 mg/mL IL-2 in HBS-EP and 100 µL 10 mM Acetate pH 5.5) for 75 seconds, monitor binding for desired RUs. Switch back to flows one and two with a flow rate of 19 µL per minute, inject $EtOHNH_2$ for seven minutes. Stop manual run. Repeat the same protocol over flow cells three and four. Record all RU changes in the baseline and watch for air spikes and unusual binding curves.

Using the Wizard/Method Builder program in the Biacore T100 software, write a Method. Our method was written for a kinetic series of injections. We started with three start up cycles and followed with a series of 10 concentrations of our drug/NP conjugates being injected for 120 seconds with a 600 second dissociation time, all of these cycles were run in triplicate. All of the standard regeneration solutions were experimented with for this system but none successfully broke the drug/NP and IL-2 interaction without damage to the IL-2 surface, therefore we exploited a natural dissociation simply running with buffer.

All sensograms were analyzed with Bia evalution software and reported above.

References

1. Renfrey, S. and J. Featherstone, *Structural proteomics.* Nature Reviews Drug Discovery, 2002. **1**(3): p. 175-176.

2. Anderson, N. *The human plasma proteome - History, character, and diagnostic prospects.* Molecular and Cellular Proteomics, 2002. **1**(11): p. 845-867.

3. Yin, H. and A. Hamilton, *Strategies for targeting protein-protein interactions with synthetic agents.* Angewandte Chemie - International Edition, 2005. **44**(27): p. 4130-4163.

4. Fazal, M.A., et al., *Surface recognition of a protein using designed transition metal complexes.* Journal of the American Chemical Society, 2001. **123**(26): p. 6283-6290.

5. Leung, D.K., Z.W. Yang, and R. Breslow, *Selective disruption of protein aggregation by cyclodextrin dimers.* Proceedings of the National Academy of Sciences of the United States of America, 2000. **97**(10): p. 5050-5053.

6. You, C.C., et al., *Tunable inhibition and denaturation of alpha-chymotrypsin with amino acid-functionalized gold nanoparticles.* Journal of the American Chemical Society, 2005. **127**(37): p. 12873-12881.

7. Burgess, K., *Solid-phase syntheses of beta-turn analogues to mimic or disrupt protein-protein interactions.* Accounts of Chemical Research, 2001. **34**(10): p. 826-835.

8. You, C., M. De, and V. Rotello, *Mono layer-protected nanoparticle-protein interactions.* Current Opinion in Chemical Biology, 2005. **9**(6): p. 639-646.

9. Rosi, N. and C. Mirkin, *Nanostructures in biodiagnostics.* Chemical Reviews, 2005. **105**(4): p. 1547-1562.

10. Love, J., et al., *Self-assembled monolayers of thiolates on metals as a form of nanotechnology.* Chemical Reviews, 2005. **105**(4): p. 1103-1169.

11. Goodman, C. and V. Rotello, *Biomacromolecule surface recognition using nanoparticles.* Mini-Reviews in Organic Chemistry, 2004. **1**(1): p. 103-114.

12. Daniel, M. and D. Astruc, *Gold nanoparticles: Assembly, supramolecular chemistry, quantum-size-related properties, and applications toward biology, catalysis, and nanotechnology.* Chemical Reviews, 2004. **104**(1): p. 293-346.

13. Feldheim, D.L. and C.A. Foss, *Metal nanoparticles: synthesis, characterization, and applications*. 2002, New York: Marcel Dekker. ix, 338 p.

14. Templeton, A., M. Wuelfing, and R. Murray, *Monolayer protected cluster molecules.* Accounts of Chemical Research, 2000. **33**(1): p. 27-36.

15. Tamarkin, L. and G. Paciotti, *Composition and method for delivery of biologically-active factors.* US Patent 6,274,552, 1997.

16. Waldmann, T., *The IL-2/IL-2 Receptor System - A Target for Rational Immune Intervention.* Immunology Today, 1993. **14**(6): p. 264-270.

17. Campara, M.a.T.I.G.a.O., Jose, *Interleukin-2 receptor blockade with humanized monoclonal antibody for solid organ transplantation.* Expert opinion on biological therapy, 2010. **10**(6): p. 959-969.

18. Tilley, J., et al., *Identification of a small molecule inhibitor of the IL-2/IL-2R alpha receptor interaction which binds to IL-2.* Journal of the American Chemical Society, 1997. **119**(32): p. 7589-7590.

19. Arkin, M., et al., *Binding of small molecules to an adaptive protein-protein interface.* Proceedings of the National Academy of Sciences of the United States of America, 2003. **100**(4): p. 1603-1608.

20. Braisted, A., et al., *Discovery of a potent small molecule IL-2 inhibitor through fragment assembly.* Journal of the American Chemical Society, 2003. **125**(13): p. 3714-3715.

21. Raimundo, B., et al., *Integrating fragment assembly and biophysical methods in the chemical advancement of small-molecule antagonists of IL-2: An approach for inhibiting protein-protein interactions.* Journal of Medicinal Chemistry, 2004. **47**(12): p. 3111-3130.

22. Emerson, S.D., et al., *NMR characterization of interleukin-2 in complexes with the IL-2R alpha receptor component, and with low molecular weight compounds that inhibit the IL-2/IL-R alpha interaction.* Protein Science, 2003. **12**(4): p. 811-822.

23. Brust, M., et al., *Synthesis And Reactions Of Functionalized Gold Nanoparticles.* Journal Of The Chemical Society-Chemical Communications, 1995(16): p. 1655-1656.

24. Brust, M., et al., *Synthesis of Thiol-Derivatized Gold Nanoparticles In A 2-Phase Liquid-Liquid System.* Journal of the Chemical Society-Chemical Communications, 1994(7): p. 801-802.

25. Ackerson, C.J., et al., *Synthesis and Bioconjugation of 2 and 3 nm-Diameter Gold Nanoparticles.* Bioconjugate Chemistry. **21**(2): p. 214-218.

26. Ackerson, C.J., et al., *Rigid, specific, and discrete gold nanoparticle/antibody conjugates.* Journal of the American Chemical Society, 2006. **128**(8): p. 2635-2640.

27. Rich, R.L. and D.G. Myszka, *Grading the commercial optical biosensor literature-Class of 2008: 'The Mighty Binders'.* Journal of Molecular Recognition. **23**(1): p. 1-64.

Appendix

Absorbance profiles for compounds **3** and **4** as well as for **2.0 nm gold particles :**

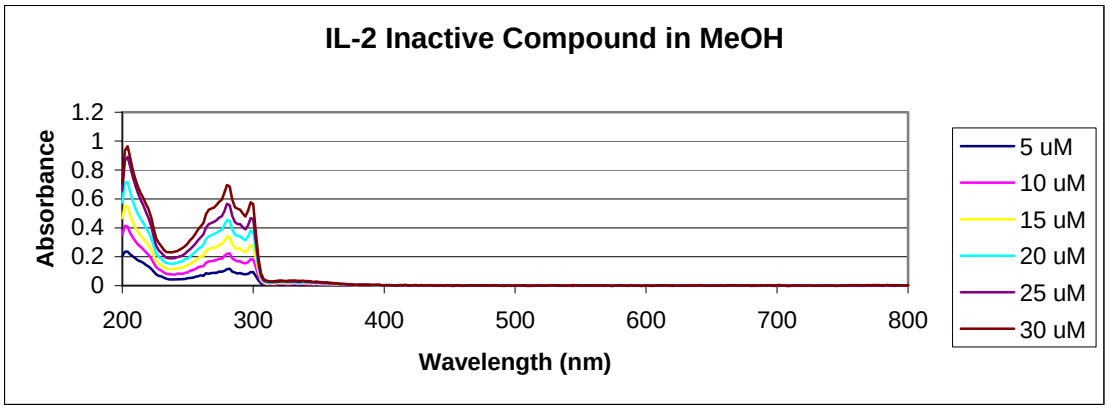

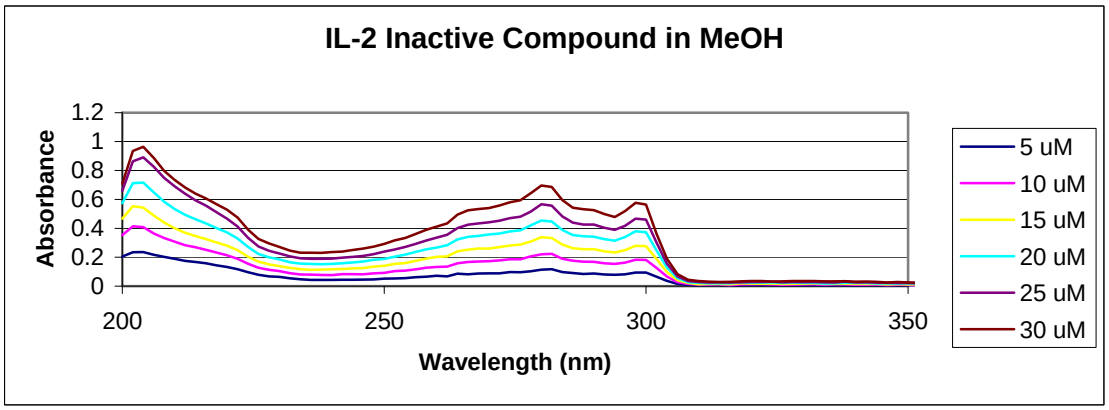

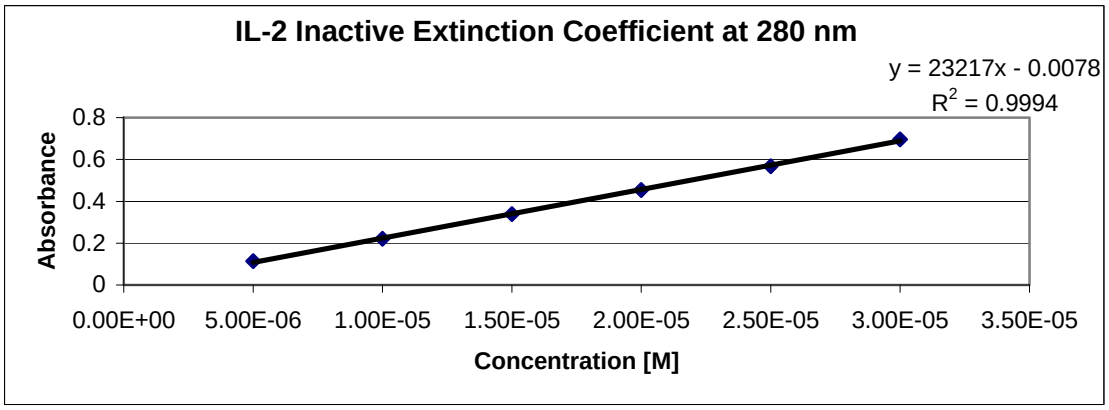

Figure A1. Absorbance Profile and Extinction Coefficient for IL-2 Inactive Compound

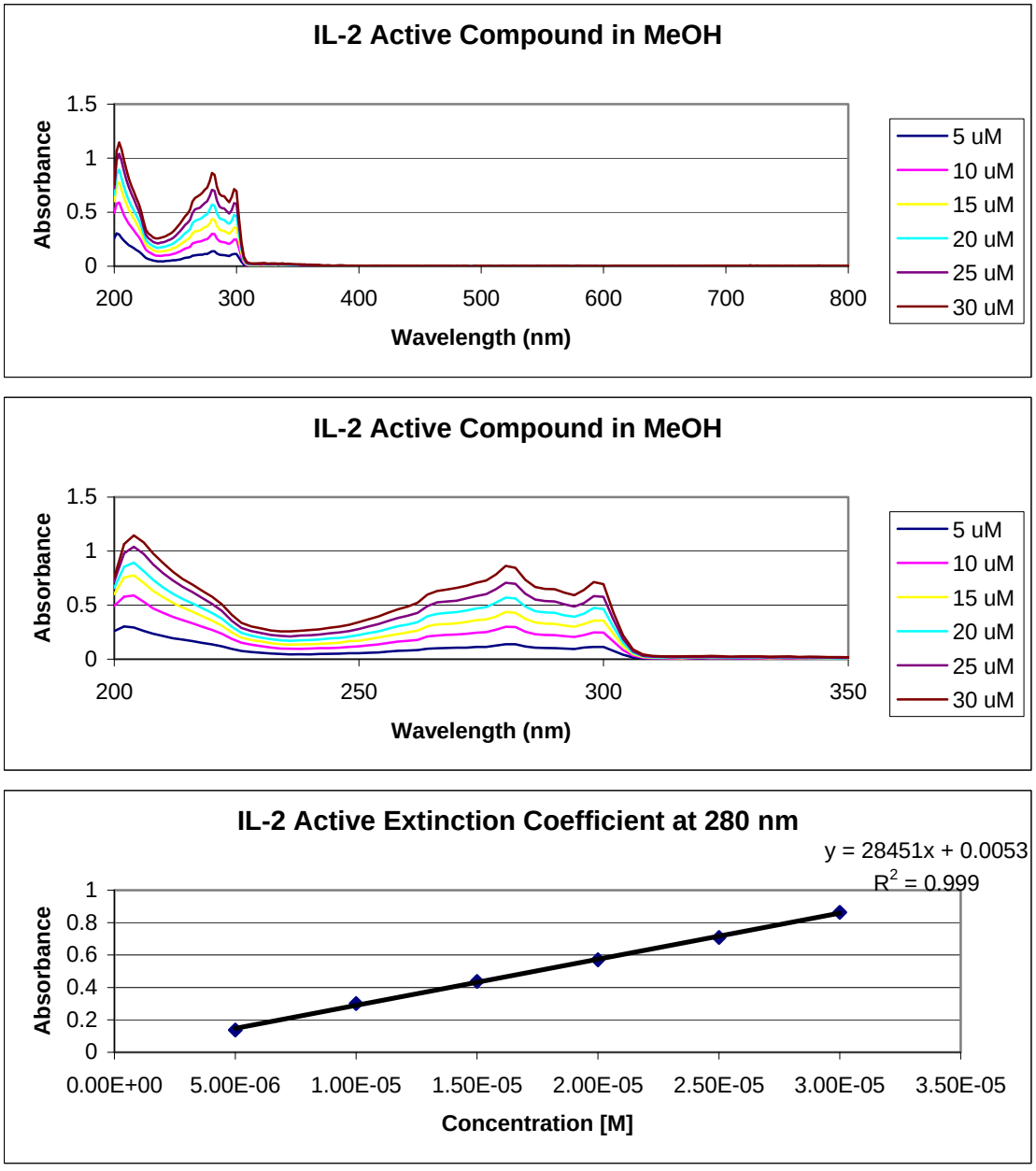

Figure A2. Absorbance Profile and Extinction Coefficient for IL-2 Active Compound

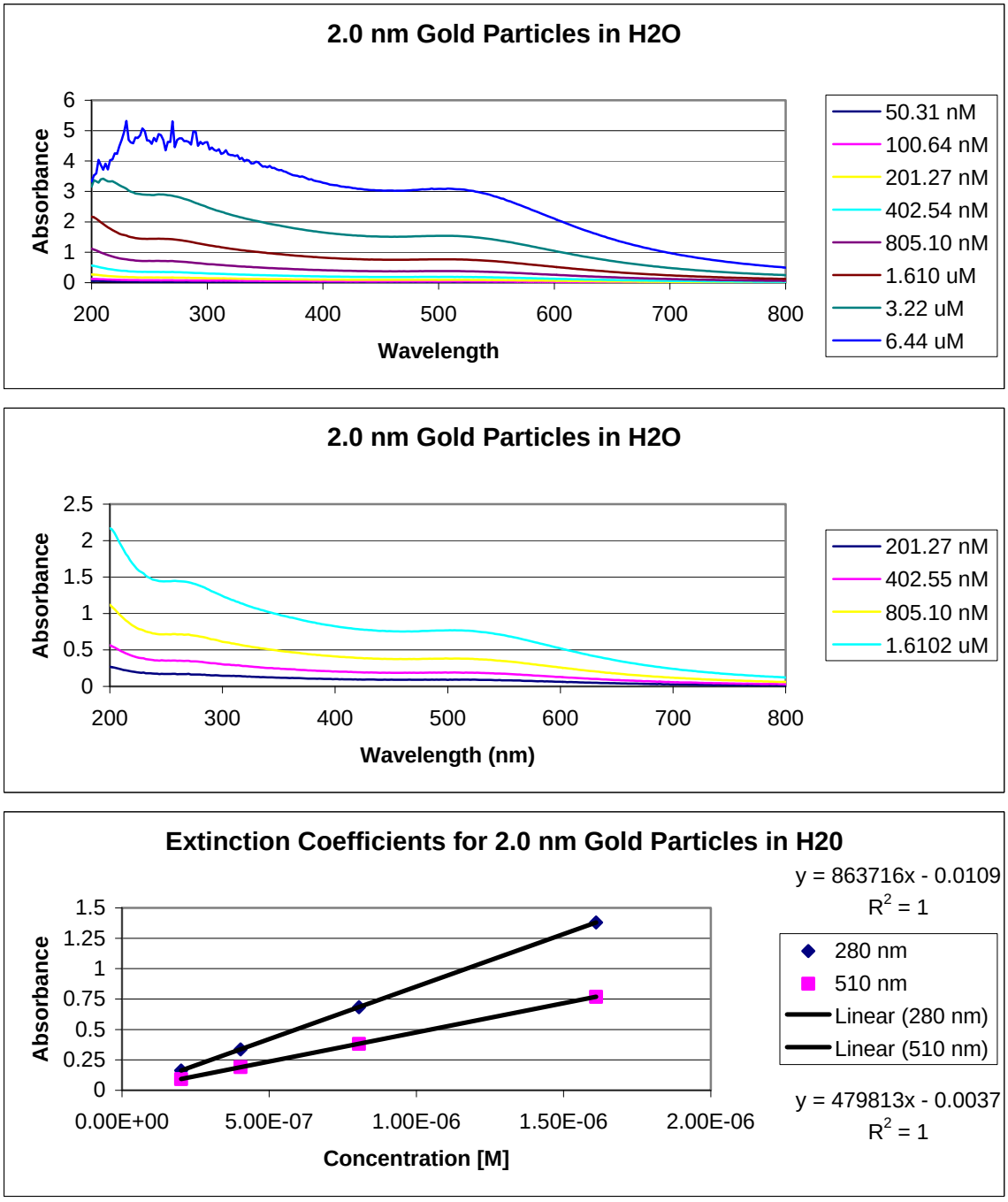

Figure A3. Absorbance Profile and Extinction Coefficient for 2.0 nm gold particles.

Background on Biacore

Biacore was founded in 1984 and was purchased by GE in 2006. The instruments have gone through generations of improvements, both hardware and software updates. Biacore enables a label free, real time detection and monitoring of biomolecular binding events utilizing three key technologies, Surface Plasmon Resonance (SPR), microfluidics and the gold dextran surface of the sensor chip as depicted in **Figure A4**.

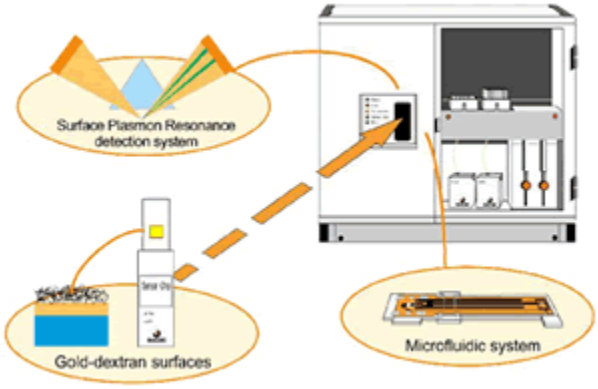

Figure A4. The Three Integral Components of Biacore

The key component of Biacore is the sensor chip. The chip is a thin layer of gold modified with a carboxymethylated dextran layer that allows attachment of one of the binding partners to the chip surface. The chip is divided into four flow cells; the division of flow cells allows for four separate experiments to occur simultaneously. Biacore also employs a microfluid system that allows consistent and continuous flow of buffer over all flow cells of the sensor chip. The constant flow of buffer allows the mobile phase (drug/AuNP conjugates) to move and preserves the stationary phase (IL-2). The thin gold

layer of the sensor chip sets an ideal stage for SPR, which acts as the detector. SPR measures changes in the refractive index of incident polarized light on the back of the sensor chip, thus detecting changes in mass of the ligand in the aqueous layer close to the sensor chip surface. The change in the refractive index is shown by response units (RU) on a sensogram (**Figure A5**). Biacore instruments are highly sensitive; therefore when operating one you must pay special attention to the optimization of several experimental parameters, including ligand immobilization (desired RU and method or immobilization), surface regeneration conditions, as well as analyte concentrations, buffer, and injection/dissociation times. A sensogram gives information about the binding affinity and kinetics in real time.

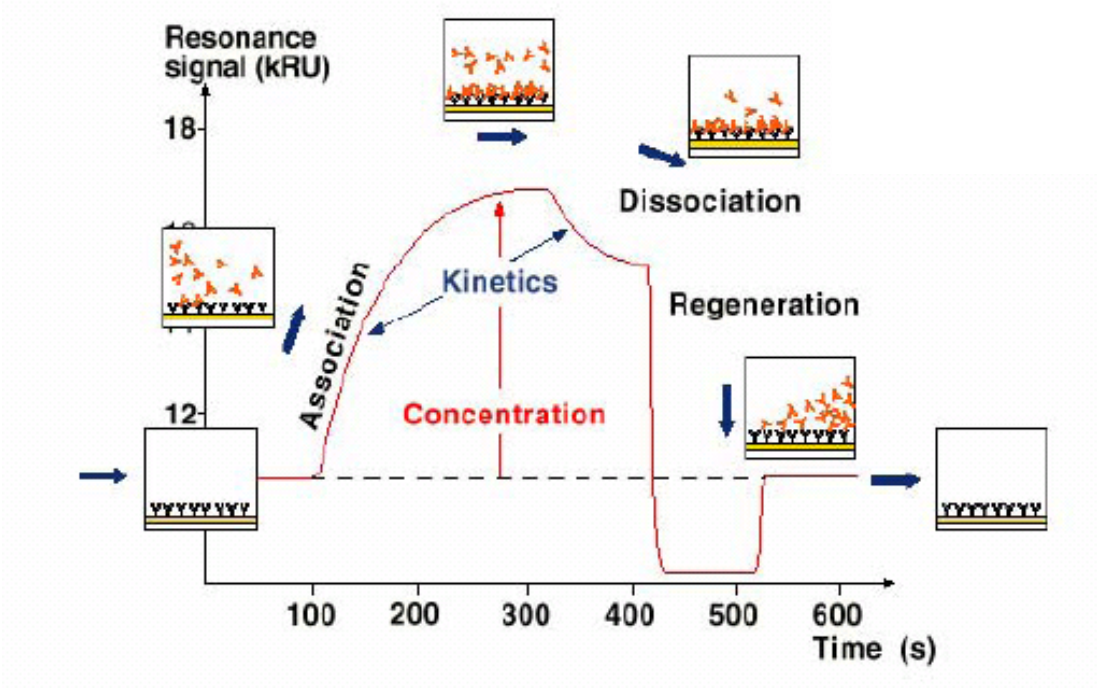

Figure A5. Basics of a Sensogram

There are two analytical methods for determining affinity constants from Biacore data. One method is by determining a kinetic on/off rate by fitting the data to a theoretical model, and dividing the off rate by the on rate to get a K_d. The other method is by fitting steady state binding data to a theoretical isotherm.

Application of Biacore for the study of polyvalent interactions is common, but it is typically used for showing qualitative binding, not extracting quantitative numbers. This is because any kinetic model for modeling a polyvalent interaction must assign a separate k_a and k_d for each monovalent interaction within the polyvalent interaction. For polyvalent interactions with more than a few interacting components, this is difficult. There are a few examples in the literature of quantitative models for considering kinetics of polyvalent binding on an SPR surface, but they are not yet widely used, with the exception of antibody (bivalent analyte) models.